Development of
Brain-Mimetic Hydrogels
For Modelling Neuronal Differentiation

by

Duygu Turan Sorhun

A Dissertation Submitted to the
Graduate School of Health Sciences
in Partial Fulfillment of the Requirements for
the Degree of

Master of Science

in

Cellular and Molecular Medicine

December 30, 2022

Development of
Brain-Mimetic Hydrogels
For Modelling Neuronal Differentiation

Koç University

Graduate School of Health Sciences

This is to certify that I have examined this copy of a master's thesis by

Duygu Turan Sorhun

and have found that it is complete and satisfactory in all respects,
and that any and all revisions required by the final
examining committee have been made.

Committee Members:

_____

Assist. Prof. Dr. Ece Öztürk (Advisor)

_____

Assoc. Prof. Dr. Atay Vural

_____

Assoc. Prof. Dr. Duygu Ege

Date: January 18th ,2023

Dedicated to all suffering from neurodegenerative diseases…

ABSTRACT

Development of Brain-Mimetic Hydrogels for Modelling Neuronal Differentiation

Duygu Turan Sorhun

Master of Science in Cellular and Molecular Medicine

December 30, 2022

Biomechanically and biochemically tunable brain tissue models are notably essential for tissue engineering applications and neuroscience studies. Derivation of hydrogels through decellularization of native tissues is a promising strategy to reconstitute the native brain extracellular matrix for use in *in vitro* human models. Due to distinct features of the brain tissue and its implications on cellular behavior, it is particularly important to characterize and modulate the biochemical and biomechanical properties of constructed hydrogels from decellularized tissues.

In the present study, we investigated the use of bovine brain tissue as a biomaterial carrier for neuroscience studies, assessed whether it could be an advantageous replacement for the human brain with easy accessibility, reproducibility and microenvironmental resemblance. We established and examined different methods for decellularization of bovine brain tissue and fabrication of reconstituted hydrogels. The decellularized tissues were evaluated with histological assessments and biochemical assays to both confirm elimination of cellular material and conservation of extracellular matrix components.

Afterwards, decellularized tissues were solubilized with enzymatic digestion and reconstituted under physiological conditions in order to form hydrogels with thermal crosslinking capability. Mechanical characterization of hydrogels was performed to assess their stiffness and viscoelastic properties. Hydrogels were then tested for their three-dimensional cell encapsulation efficiency and their cytocompatibility with neuroblastoma cell line (SH-SY5Y) in culture. Collectively, it was shown that each decellularization technique resulted in different biochemical and biomechanical properties and these factors affected cell growth and behavior such as the degree of neurite formation. Given that mechanical microenvironment acts as an important parameter in cancer and neurodegenerative diseases, the results of this study provide significant insights.

In the second part of the study, neuronal differentiation of neuroblastoma cells was investigated under 2D and 3D cell culture conditions to assess the effect of culture dimensionality and the presence of native brain matrix ligands on cellular fate. For this purpose, neuroblastoma cells were either grown on cell culture plate or encapsulated within decellularized brain-derived hydrogels. Following a neuronal differentiation regime, cells were evaluated morphologically through brightfield microscopy to determine neurite formation. Then, the expression of neuronal markers was assessed on both protein level by immunostainings and gene level by qRT-PCR. In conclusion, it was shown that synaptogenesis was improved by differentiated cells with elongated neurite formation in both 2D and 3D cultures. The proliferation rate was reduced and the gene expression levels of neuronal markers, including *TUBB3* and *CHAT* were increased. Besides the common trends, significant differences were also observed between 2D and 3D cultured differentiated cells, whereas in 3D culture an increase in *GFAP,* glial cell marker, was detected.

ÖZETÇE

Nöronal farklılaşmayı modelllemek için beyin-mimetik hidrojel geliştirilmesi

Duygu Turan Sorhun

Hücresel ve Moleküler Tıp, Yüksek Lisans

December 30, 2022

Biyomekanik ve biyokimyasal olarak ayarlanabilir beyin dokusu modelleri, doku mühendisliği uygulamaları ve nörobilim çalışmaları için özellikle önemlidir. Doğal dokuların hücresizleştirilmesi yoluyla hidrojellerin türetilmesi, *in vitro* insan modelleri kullanımında doğal beyin hücre dışı matrisini yeniden oluşturmak için umut verici bir stratejidir. Beyin dokusunun farklı özellikleri ve hücresel davranış üzerindeki etkileri nedeniyle, hücresizleştirilmiş dokulardan yapılan hidrojellerin biyokimyasal ve biyomekanik özelliklerini karakterize etmek ve modüle etmek özellikle önemlidir.

Bu çalışmada, sığır beyin dokusunun nörobilim çalışmaları için bir biyomateryal taşıyıcı olarak kullanımını araştırdık, ve kolay erişilebilirlik, tekrarlanabilirlik ve mikro-çevresel benzerlik ile insan beyninin yerine avantajlı bir tercih olup olamayacağını değerlendirdik. Sığır beyin dokusunun hücresizleştirilmesi ve hidrojellerin üretimi için farklı yöntemler belirledik ve inceledik. Hücresizleştirilmiş dokularda, hem hücresel materyalin ortadan kaldırıldığını hem de hücre dışı matris bileşenlerinin korunduğunu doğrulamak için histolojik değerlendirmeler ve biyokimyasal deneyler yapıldı.

Daha sonra hücresizleştirilmiş dokular, enzimatik sindirim ile çözündürüldü ve termal çapraz bağlanma kabiliyetine sahip hidrojelleri oluşturmak için fizyolojik koşullar altında yeniden yapılandırıldı. Sertliklerini ve viskoelastik özelliklerini değerlendirmek için hidrojellerin mekanik karakterizasyonu yapıldı. Hidrojeller daha sonra üç boyutlu hücre kapsülleme etkinlikleri ve kültürde nöroblastoma hücre dizisi (SH-SY5Y) ile hücre uyumluluğu açısından test edildi. Toplu olarak, her hücresizleştirme tekniğinin farklı biyokimyasal ve biyomekanik özelliklerle sonuçlandığı ve bu faktörlerin hücre büyümesini ve nörit oluşum derecesi gibi davranışları etkilediği gösterilmiştir. Mekanik mikroçevrenin kanser ve nörodejeneratif hastalıklarda önemli bir parametre olarak değişim gösterdiği göz önüne alındığında, bu çalışmanın sonuçları önemli bilgiler vermektedir.

Çalışmanın ikinci bölümünde, kültür boyutluluğunun ve doğal beyin matris ligandlarının varlığının hücresel etkisini değerlendirmek için nöroblastoma hücrelerinin nöronal farklılaşması, 2B ve 3B hücre kültürü koşulları altında araştırıldı. Bu amaçla, nöroblastoma hücreleri ya hücre kültürü plakası üzerinde büyütüldü ya da hücresizleştirilmiş beyin kaynaklı hidrojeller içinde kapsüllendi. Bir nöronal farklılaşma rejiminin ardından hücreler, nörit oluşumunu belirlemek için ışık mikroskobu yoluyla morfolojik olarak değerlendirildi. Daha sonra, nöronal belirteçlerin ekspresyonu hem protein seviyesinde immün boyamalarla hem de gen seviyesinde qRT-PCR ile değerlendirildi. Sonuç olarak, hem 2B hem de 3B kültürlerde uzun nörit oluşumu ile farklılaşmış hücreler tarafından sinaptogenezin iyileştirildiği gösterilmiştir. Çoğalma hızı azalmakta ve *TUBB3* ve *CHAT* dahil olmak üzere nöronal belirteçlerin gen ekspresyon seviyeleri artmaktadır. Gözlemlenen ortak eğilimlerin yanı sıra, 2B ve 3B kültürlü farklılaşmış hücrelerde de önemli farklılıklar gözlenirken, 3B kültürde glial hücre belirteci olan *GFAP*'de bir artış tespit edildi.

AKNOWLEDGEMENTS

First of all, I would like to thank my advisor, Dr. Ece Öztürk, for her trust and support. We became a light for each other on an unknown brain model development journey that she and I set out and our journey ended up with great success. I feel joyful about being her first graduate student. Another factor in achieving these successes is my previous PIs Ezgi and Hüseyin Abdik, who believed in me during my bachelor's study and improved me with great devotion. I would like to thank each of them for their support in projects.

Of course, the effects of this journey were not limited to the laboratory. I had very important supporters during this adventure and the first and foremost person was my partner Ömer Emre Sorhun. He listened to all my problems within the experiments, even though he tried to troubleshoot with me. He taught me how to be strong and not to fail when conferring a problematic situation. My mom and dad, Özlem-Hamdi Turan, and my brother Oktay Turan back me up unconditionally in each stage of my life and I stand up with their support and love. I would like to express my endless thanks to Sacide and İsmail Sorhun for always wanting the best for me. I also want to thank another very valuable person in my life, my sister, Simay Karaman, not only for her support in last 2 years but also in my whole life since 2007. Doruk Anıl, my precious friend, also helped me a lot in this time of period. I also want to thank Çıtır, my dog, and Barney, my cat, for not eating my thesis and not breaking my PC. I feel so lucky to have each of them.

I am very pleased to make acquainted with ECO-lab members. I would like to thank Deniz Örnek, for her support not only in lab, but also outside the boundaries of the school. We collected so many good memories together and she was my best partner-in-crime. I would like to thank especially Alican Kuşoğlu for his support in this project. I do not feel alone in this project by his contributions. Lastly, I would like to share my thanks to Sevgi Sarıca, Kardelen Yangın. Sena Özkan, Nuriye Solcan, and Şevval Özdinç for their valuable friendship.

TABLE OF CONTENTS

TABLE OF CONTENTS

LIST OF TABLES

LIST OF FIGURES

ABBREVIATIONS

2D	two dimensional
3D	three dimensional
APP	amyloid-beta precursor protein
CHAT	choline o-acetyltransferase
DAPI	4',6-diamidino-2-phenylindole
db-ECM	decellularized brain extracellular matrix
DMEM	Dulbecco's modified eagle's medium
DNAse	deoxyribonuclease
ECM	extracellular matrix
EDTA	ethylenediaminetetraacetic acid
FBS	fetal bovine serum
GAPDH	glyceraldehyde-3-phosphate dehydrogenase
GFAP	glial fibrillary acidic protein
MAP2	microtubule-associated protein 2
MAPT	microtubule associated protein tau
NEUN	neuronal nuclei
P/S	penicillin/streptomycin
PBS	phosphate buffered saline
PG	proteoglycan
PSEN1	presenilin 1
RA	retinoic acid
RET	ret proto-oncogene
RT-q-PCR	reverse transcription quantitative real-time PCR
SDC	sodium deoxycholate
SDS	sodium dodecyl sulfate
sGAG	sulphated glycosaminoglycan
SOX2	SRY-Box transcription factor 2,
SYP	synaptophysin
TUBB3	beta-tubulin III

Chapter 1: **INTRODUCTION**

1.1 The Extracellular Matrix

The extracellular matrix (ECM) is the fundamental non-cellular unit found in all tissues. The main components of ECM include macromolecules such as proteoglycans (PGs), fibrous proteins, such as collagens, elastins, laminins, and fibronectins, and water [1]. The ECM arranges physical scaffolding and sets the ground for intercellular interactions in addition to biochemical reaction chains required for homeostasis, migration, differentiation, and several specific functions. During the development of the cellular microenvironment, each tissue attains a unique composition and topology within its ECM. In addition to the distinctions in different tissue types, alterations such as aging, wounding or disease progression lead to dynamic changes in the ECM composition and organization [2, 3].

1.1.1 Brain Extracellular Matrix

Extracellular matrix (ECM) covers approximately 10-20% of the brain volume and it performs important functions within the central nervous system. The first and main function, that brain ECM covers is the construction of a biological scaffold. Apart from being a biological scaffold, it also creates a physical barrier that controls the diffusion of molecules. Moreover, it regulates the biomechanical properties by the aid of molecular interactions. It has a major impact on nervous system development, thereby promoting cell migration, differentiation, neurite outgrowth, and synaptogenesis. It controls neuronal network remodeling, production, spread of neurotrophic factors, and synapse stability [4]. The brain is distinguished from the other organs by its outstanding features, such as limited stromal space with well-defined ultrastructure [5] and the low amount of fibrous ECM proteins including fibronectin, vitronectin, and collagen, which are frequently encountered in other organs. Furthermore, the ratio between the amount of glycosaminoglycans (GAGs) to collagen in brain ECM remains 10:1 [6-8]. GAGs can be encountered either in unbounded form as hyaluronan or protein-bound form as proteoglycans, such as chondroitin sulphate proteoglycan or heparan sulphate proteoglycan [4].

As shown in *Figure 1*, the adult brain ECM can be divided into three separate compartments and these are the basement membrane, the perineuronal nets, and the neural interstitial matrix. The basement membrane environing the central nervous parenchyma surrounds vascular structures, mainly cerebral vessels. It contains mainly collagen, laminin–nidogen(entactin) complexes, dystroglycan, fibronectin, and perlecan. Apart from the formation of the non-cellular unit of the blood-brain barrier, it also plays role in cell polarity and differentiation [4, 9]. The perineuronal nets are in the form of a lattice-like matrix including hyaluronan, chondroitin sulfate proteoglycans, tenascin R, and link proteins. This matrix not only protects neuronal cells by directly covering the neuronal cells, but also has a role in synaptic plasticity, regulation of ion homeostasis, and stabilization of synapses [10]. There are different proteoglycans present in the brain ECM and they are mostly dispersed in the intercellular spaces between neuronal and glial cells, which creates the third matrix type. The neural interstitial matrix includes proteoglycans, hyaluronan, tenascins, and link proteins. This compartment also contains fibrous proteins (collagens and elastin) and adhesive glycoproteins (laminins and fibronectins) in small portions [11]. This section of the brain ECM provides tissue hydration and promotes tissue integrity [4]. Apart from its macroscopic and microscopic heterogeneous complex ultrastructure, it also has outstandingly complex mechanical response [12].

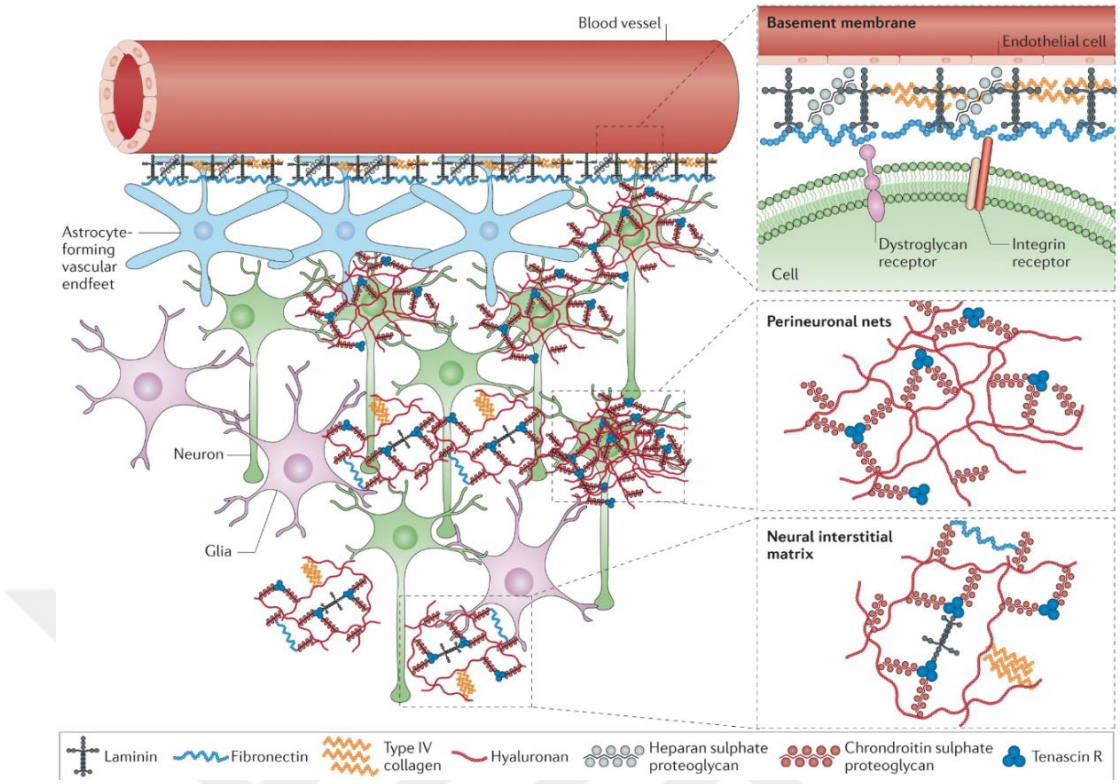

Figure 1 Scheme showing brain ECM components. Figure retrieved and adapted from Lau *et.al.* 2013 with permission [11].

1.1.2 Bovine Brain vs Human Brain

Bovine (*Bos taurus*) brain tissue is a promising source for brain ECM studies in the field of neuroscience. The bovine brain has high similarity to the human brain with its large size and gyrencephalic structure, which is the state of folding and convolutions within the cerebral cortex. As an organism, humans and bovines have also similar characteristics of gestation time which is approximately 40 weeks. Another advantage of using the bovine brain in 3D culture experiments is its easy accessibility from local slaughterhouses [13]. Recently, various bovine tissues, such as ovarian tissue [14], flexor tendons [15], retina [16], and spinal cord meninges [17], were used as a source in decellularization procedures to fabricate hydrogel or ECM carriers. However, based on literature review, there were not any studies published for bovine brain decellularized tissue-derived hydrogel and characterization of the decellularized bovine brain tissue. Exceptionally, in Beachley's *et.al*. study, decellularized white and gray matter of the bovine brain were used separately to construct a multi-tissue core–shell Hyaluronic acid–ECM hydrogel in order to demonstrate neuronal differentiation [18].

1.2 Three-dimensional tissue models

Nowadays, for molecular biology and biotechnological applications, three-dimensional tissue models are more convenient and favorable than two-dimensional cultures and *in vivo* studies [3]. More particularly, 2D cell culture models are not sufficient to display key aspects of the brain microenvironment in terms of supporting cellular processes such as synaptogenesis, differentiation, neurodevelopmental processes, neuronal maturation processes, and cell-cell signaling pathways [19]. 2D platforms are not limited by a physical barrier, so there is a lack of boundaries, and cell spreading and adhesion are polarized as shown in *Figure* 2. ECM stiffness, which has a much higher degree in 2D culture conditions in comparison to 3D matrices, is sensed by applied inward traction forces by cells. On the other side, 3D platforms are restricted with a defined space, so cell spreading, migration, and cellular growth occur on a limited scale. Mostly, the stiffness and mechanical properties can be modulated within the 3D matrices and mechanotransduction can be affected by several physical forces including compression and degradability [20, 21].

To mimic molecular systems or diseases in three dimensions, natural or synthetic polymers can be used [21]. Decellularization, which is the preservation of ECM by removal of any cellular and nuclear components from a tissue, is one of the most frequently applied methods to generate three-dimensional tissue models [22]. Considering the composition and the properties of the tissue of interest, the decellularization process should be optimized to modulate the related tissue parameters. By a broad classification, physical, chemical, and biological decellularization methods can be performed and each treatment has a different impact on the tissue composition. The operated decellularization method should therefore be determined carefully, especially for delicate tissue types, such as brain tissue [23].

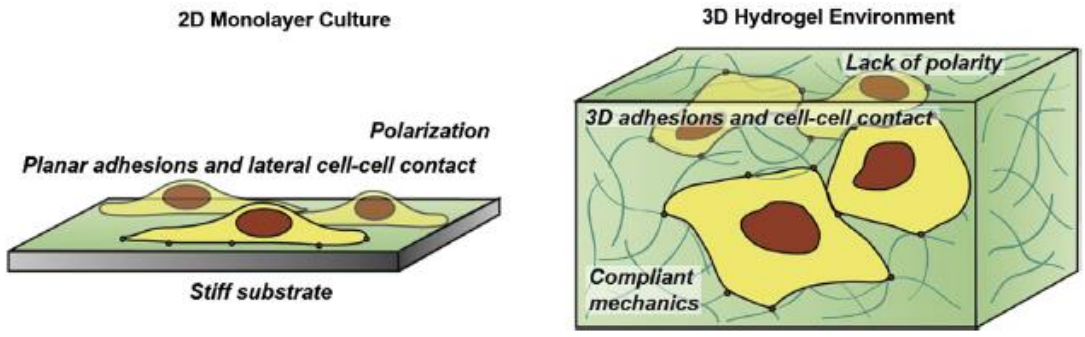

Figure 2 Comparison of 2D and 3D cell culture Figure retrieved and adapted from Wilson *et.al.* 2017 with permission [21].

1.2.1 Decellularization

Physical decellularization methods involve freeze-thaw, mechanical force such as high hydrostatic pressure, mechanical agitation, and supercritical carbon dioxide treatment [24]. Chemical treatments compromise non-ionic detergents such as Triton X-100, ionic detergents such as sodium dodecyl sulfate (SDS), sodium deoxycholate (SDC), or Triton X-200, hypotonic and hypertonic solutions, acids and bases including peracetic acid or ammonium hydroxide. Lastly, the biological approach comprises the use of enzymes including trypsin, dispase, endonucleases such as DNAse, and exonucleases. The role of DNAse is especially important in order to prevent immunological reactions by removing DNA fragments larger than 200 bps and the total DNA content in the ECM-based materials should be less than 50 ng double-stranded DNA per mg ECM dry weight [24, 25]. During engineering biological scaffolds, it is important to design decellularization methods addressing the specific properties of the studied tissue and the lipid content is one of them. Tissues including the pancreas, brain, and adipose have high lipid content, therefore, delipidation steps should be adopted within the decellularization process. Regarding brain tissue decellularization, there is a lack of studies in which delipidation process was adapted [26]. Eventually, the ultimate goal for an optimized decellularization methodology is the maximum cell removal rate with minimum ECM damage [27].

1.2.2 Hydrogel construction

Hydrogels derived from decellularized brain tissue are promising models to mimic the brain microenvironment [28]. The major steps in hydrogel formation are the

solubilization process of the d-ECM powder into protein monomeric components and the neutralization process. There are different methods for solubilization, thus, the frequently applied method is Freytes, in which 1 mg/ml pepsin in 0.01M HCl and the d-ECM powder are stirred at room temperature[29, 30]. Afterwards the digest is neutralized to achieve the physiological pH and salt conditions [31].

There are several advantages of such hydrogels, but, the most important one is the conservation of biochemical complexity within the d-ECM hydrogels [31]. After the decellularization procedure, the significant part of the ECM components is retained, so the microenvironment demonstrates the capability of recapitulating the native tissue itself [28]. Mostly, this beneficial property cannot be provided by other polymers used for tissue modelling. However, besides their advantages, there are several points to be considered. For instance, sterilization of decellularized tissues is a challenge to be addressed and the risk of pathogen transfer should be eliminated [22]. Another important factor to consider is maintaining mechanical stability as it is a major difficulty in decellularized matrix-derived hydrogels. To overcome this difficulty, detailed characterization of d-ECM hydrogels comprising important factors, such as polymer content, changes in ECM proteins according to the applied decellularization methods, and biomechanical properties including stiffness and viscoelasticity is critical [32]. For this reason, mimicking such a delicate tissue requires fully characterized scaffolds and the ability to modulate several parameters on that scaffold [8].

1.3 Mechanical characteristics regarding tissue models

The brain, possessing a very soft structure, is confined within the skull which acts as a hard boundary for protection [10]. Rodent and human brain tissue exhibit viscoelastic behavior with Young's modulus alternating between 0.1-16 kPa [33]. Neuronal cells prefer soft platforms such as ~700 Pa for growth and maturation, but too soft materials are also hampering neurons to extend their neurites. Mechanotransduction aids the conversion of the physical forces and mechanical stimulus into biochemical signaling pathways using membrane-bound mechanosensory components within the cells [10].
There are studies demonstrating the changes in elasticity and viscoelasticity of the aging or diseased brain tissue [34-36]. For instance, it has been shown that there is reduced stiffness and viscosity in the hippocampus of Alzheimer's disease patients [37].

Moreover, the reduction of viscoelasticity was also observed in multiple sclerosis patients' brains [34, 38]. The implications of such findings for ECM-related biomechanical changes reveal the importance of the need for mechanically controllable scaffolds. Therefore, an elaborative mechanical characterization of d-ECM hydrogels presents an essential need in the field.

1.4 Literature review for decellularized brain models

To date, there is not any published study regarding derivation of decellularized bovine brain-ECM derived hydrogels. In DeQuach et al.'s study, the porcine brain tissue was decellularized using SDS detergent and further processed to be used as a coating material for human induced pluripotent stem cells-derived neuron culture. It was claimed that the produced matrix contains various collagen isoforms, laminin, and perlecan and is rich in GAGs [39]. From another perspective, several studies stated that treating tissues with detergent might pose a risk to the gelation kinetics during hydrogel formation. Consequently, during decellularization, the concentration choice of the SDS plays a very important role [40-42]. However, in DeQuach et al.'s study, the generation of hydrogel was successfully achieved, supporting neuronal growth, and having a proper gel form with minimum cellular content. Sood et al. developed another model to show the support of fetal porcine brain ECM on neural growth and differentiation. This model involves a donut-shaped structure to mimic the white matter at the center and the grey matter in the surrounding. Slight changes in chemicals were applied during the decellularization of the adult and fetal porcine brains, so they also compared the adult and fetal brain constructs and their impact on neuronal growth [6]. In a further study done by Jung et al., composite brain hydrogels were constructed using decellularized porcine brain tissue and anisotropic orientation was achieved. They argued that in this way the brain was mimicked better anatomically and consequently neuronal network was enhanced with augmented dynamic signalling [43]. Lastly, Koh et.al. articulate in their work how to recapitulate the glioblastoma microenvironment using patient-derived decellularized brain tissue. They argued that using organ-specific decellularized tissues might provide a physiologically more relevant ECM microenvironment in tumor models [44].

1.5 Neuroblastoma cells and their use in brain models

The human neuroblastoma cell line, SH-SH5Y, is a subcloned epithelial cell line from SK-N-SH, which originated in 1970 from a metastatic bone tumor, which was retrieved from a 4-year-old female patient's bone marrow biopsy [45]. To obtain a homogeneous cell population with moderate levels of neurotransmitter production, the neuroblastoma cells should be differentiated according to the need within the designed experimental model.

1.6 Differentiation of neuroblastoma cells

Cell proliferation is an important characteristic of immature neuroblastoma cells, whereas the proliferation rate should be decreased after differentiation [46]. One of the main factors followed in the differentiation protocols is the gradual decrease of the fetal bovine serum in the cell culture growth medium from 10% to generally 2.5%. On the other hand, the starved cells are mostly supported with neurotrophic elements such as N2, B27, retinoic acid (RA), brain-derived neurotrophic factor (BDNF), and potassium chloride (KCl) [47]. RA, a form of vitamin A, has a key role in the differentiation of neuroblastoma cells into dopaminergic neurons by its interplay in the arrest of the cell cycle, elevated levels of cyclin-dependent kinase (CDK) inhibitors and anti-apoptotic proteins, and its promotion role in PI3K/AKT signaling cascade [48]. N2 supplement contains compounds such as insulin, transferrin, selenium, etc. which are formulated as 'Bottenstein's N-1 formulation' [49] and it promotes differential signaling at the early stages. B27 protects neuronal cells with cell survival and it also inhibits glycolysis [50].

The combination of these two applications, deprivation of serum and administration of neurotrophic factors, results in the selection of epithelial cells from the population, while differentiated mature neurons with elongated neurites are expanding. According to the differentiation protocol applied, different neuronal subtypes can be achieved including adrenergic, cholinergic, and dopaminergic neurons[51]. The differentiated cells, which are phenotypically closer to the primary neurons, have reduced proliferation rate, extended long axons connected with the surrounding cells, and polarized cell structure, while undifferentiated epithelial-like cells have larger cell soma with extended short neurites. Mature neuronal marker expressions are observable at gene and protein levels [47].

1.7 Neuronal differentiation markers

Microtubule-associated protein family members play an essential role in neurodegenerative disease progression and neuromorphogenic processes. One of these markers includes MAP2 (Microtubule-associated protein 2) which is a gene responsible for the stabilization of dendrites during neurogenesis. During neurite initiation, microtubules and F-actin proteins are reconstructed by the aid of the coordination action guided by MAP2 [52]. While MAP2 is localized to the cell soma and dendrites, the other microtubule-associated protein TAU is settled in the axonal regions. MAPT (Microtubule Associated Protein Tau) has similar functions within the neuronal cells, as it promotes microtubule rigidity during dynamic cellular events [53]. TUBB3 (class III beta-tubulin, also stated as Tuj1) is another marker localized in the neuronal cytoskeleton and increased expression of TUBB3 is present in the early stages of neuronal differentiation so it has implications on axonal maturation [54].

NEUN appeared as a neuronal nuclei marker localized within the post-mitotic neuronal nuclei and perinuclear cytoplasm beyond previously mentioned cytoskeletal markers. This marker is commonly used in studies as it is not specific to a subtype of a neuron. NEUN is expressed much more in the neuronal nuclear areas, where low chromatin density with loosely packed DNA is present [55]. SYP (Synaptophysin), an integral membrane protein, is one of the first markers detected for neuronal cell identification. It regulates synaptic vesicle endocytosis and neurotransmitter release, which is crucial for neuronal cell communication within the organism [56, 57]. The most prevailing neuronal differentiation marker retrieved from the stem cell perspective is SOX2 (SRY-Box Transcription Factor 2). The studies showed that terminal neuronal differentiation is prevented by constitutive SOX2 expression, which results in intact progenitor features. Concordantly, SOX2 expression should be downregulated during neuronal differentiation [58]. RET (Ret Proto-Oncogene) is an unordinary marker linked to early neuronal differentiation; thus, it has an impact on neural crest development. There are studies showing the upregulation of *RET* during differentiation with RA treatment [59-61].

Apart from the markers which have the potential for neuronal maturation in general, there are also genes and proteins regulating the formation of subtypes of neurons,

including dopaminergic, cholinergic, serotonergic, etc. CHAT (Choline O-Acetyltransferase) is a gene required for the production of enzymes to synthesize the neurotransmitter acetylcholine, which completes the functionality of the cholinergic neurons [62]. Apart from neuronal markers, other markers regarding oligodendrocytes or glial cells are also important for the characterization of differentiated cells. GFAP (Glial fibrillary acidic protein) is an intermediate filament-III protein and is present in astrocytes in the central nervous system, non-myelinating Schwann cells in the peripheral nervous system, and enteric glial cells [63].

On the other hand, in the study, several neuronal markers, which have no direct relationship with the neuronal differentiation process stated in the literature, were studied and these were APP (Amyloid-beta precursor protein) and PSEN1 (Presenilin 1). These two proteins are encountered mostly by the pathological events occurred in Alzheimer's Disease. Although the formation of pathological oligomers derived from APP is well-studied, the physiological role is not completely understood. However, it was stated that APP might have an important role in synaptic plasticity and the development of the brain. More particularly, it guides growing axons, regulates dendritic morphology, and promotes early nervous system development [64]. Another key player of Alzheimer's Disease pathogenesis is the PSEN1 protein, which is the section of the gamma-secretase enzyme that is responsible for the cleavage of the APP. Furthermore, PSEN1 might have a role in calcium metabolism and processing of Notch, and β-catenin along with APP [65].

1.8 Scope of the study

This study includes two main objectives, which are the construction of a hydrogel system using decellularized bovine brain tissue to recapitulate the brain microenvironment and the differentiation of neuroblastoma cells in 2D and 3D conditions. For these purposes, the following steps were proceeded: (1) to evaluate different decellularization methods with various approaches on bovine brain tissue, and for this purpose, we also adapted different decellularization methods which had not been applied to the brain tissue before (2) to characterize the biochemical composition of the ECM of decellularized tissues both quantitatively and qualitatively, (3) to process the decellularized tissues in order to generate a brain ECM derived hydrogel and (4) to

investigate the hydrogels based on their biomechanical properties including gelation kinetics, elastic modulus (stiffness), creep response (viscoelasticity) and (5) to analyze the *in vitro* cytocompatibility and cell encapsulation abilities (6) to differentiate neuroblastoma cells into a mature neuron in 2D and 3D conditions.

Eventually, these brain-specific hydrogels consisting of d-ECM provide a relevant microenvironment for neurons that are able to grow and differentiate in the recapitulated *in vivo* circumstances and conditions mimicked to the original tissue. Last but not least, we developed a mechanically tuneable decellularization pipeline and made connections through various decellularization methods with biochemical content and biomechanical properties. We characterized stiffness and viscoelasticity separately and investigated the effect of these parameters on cell morphology. By this approach, further opportunities are provided for applications of remodeling neurodegenerative diseases and tumor models in tissue engineering.

Chapter 2: **MATERIALS AND METHODS**

2.1 Decellularization and hydrogel generation

Figure 3 Graphical abstract of experimental methodology (Created with BioRender.com).

2.1.1 Decellularization methods

Fresh bovine brains taken from calves were brought from a local slaughterhouse in a sealed plastic cup on ice. After rinsing the brains with 2% Penicillin-Streptomycin (P/S) included distilled water, the cerebellum was carefully separated and the cortex of the brain tissues was dissected into small pieces ($1 \times 1 \times 1$ cm^3) with a scalpel and scissor. Seven decellularization methods were applied to each half of the brain:

A) **SDS, Triton X-100, Peracetic acid, DNAse**: The brain tissue pieces were rinsed in sterile water solutions including 2% P/S for 10 times. The brain tissues incubated in distilled water for 48 hours. Then, the tissue pieces were transferred to 0.2% SDS in phosphate buffered saline (PBS, Biowest, #L0615) solution for 24 hours and afterwards washed with PBS for 15 minutes. The following treatments were done sequentially: 40U/ml Deoxyribonuclease I from bovine pancreas (DNAse, Sigma, DN25) in 10 mM magnesium chloride ($MgCl_2$, Sigma, #M8266) buffer at pH 7.5 for 12 hours at room temperature, 0.2%Triton X-100(Sigma, #X100) in PBS for 72 hours, PBS wash for 15 minutes and 0.1% peracetic acid in 4% ethanol (Isolab, #64-17-5) for 2 hours. Lastly, the remaining tissues were washed with distilled water without P/S for 8 times. All the treatments except DNAse treatment were done at 4°C on rotator [66].

B) **SDC, Triton X-100, Sucrose, Peracetic acid, Trypsin/EDTA**: The brain tissue pieces were rinsed in sterile water solutions with 2% P/S at 4°C for 12 hours. The following treatments were done sequentially; 0.05% trypsin/EDTA (Multicell, #25300-054) in PBS at 37°C for 1 hour, 3% Triton X-100 in PBS for 1 hour, 1 M sucrose (Sigma, #S1888) for 15 minutes, distilled water for 15 minutes, 4% SDC (Sigma, #30970) in distilled water for 1 hour, 0.1% peracetic acid in 4% ethanol for 2 hours, PBS wash for 15 minutes. Lastly, the remaining tissues were washed with distilled water overnight at 4°C. All treatments were done under constant rotation [67].

C) **Freeze-thaw, SDC, Triton X-100, DNAse**: The brain tissue pieces were freeze-thawed completely in PBS for 4 times. The tissue pieces were incubated in distilled water containing 1% P/S for 72 hours at room temperature. The following treatments were done sequentially; 1% Triton X-100 in PBS for 1 hour, wash with distilled water for 30 minutes, 4% SDC in distilled water for 1 hour, wash with distilled water for 30 minutes, 40U/ml DNAse in 10 mM $MgCl_2$ buffer at pH 7.5 for 1 hour and lastly the remaining tissues were rinsed with distilled water for 3-4 hours. All treatments were done under constant rotation [68].

D) **SDC, DNAse**: The brain tissue pieces were put in a large beaker on a magnetic stirrer. The tissues were washed with distilled water for 4-5 hours at 37°C and the solution was drained over sieve. Then, 1% SDC solution was added and the solution was changed every day. After incubation of 4 days, the remaining tissues were rinsed with distilled water for 5 hours and 40 U/ml DNAse in 10 mM $MgCl_2$ buffer was added and incubated overnight. Finally, the tissue pieces were washed with distilled water for 4-5 hours with liquid changes for several time [69] .

E) **SDS, DNAse**: The method which was published in DeQuach's et.al.'s paper was applied with slight modifications. The brain tissue pieces were put in a large beaker on a magnetic stirrer and incubated in 0.1% (w/v) SDS in PBS solution with 1% P/S. The solution was changed each day and incubation lasted for 4 days. Afterwards, incubation with 40U/ml DNAse in 10 mM $MgCl_2$ buffer at pH 7.5 for 2 hours was done. The thick slurry was separated into falcon tubes and washed with distilled water with sequential centrifugation at 10.000 rpm for 5 minutes for 10 times [39].

F) **Freeze-thaw, homogenization, SDC:** The brain tissues were frozen at -80°C and thawed at 37°C. Then, the tissue pieces were washed with PBS for 30 minutes,

washed with distilled water and homogenized in water until becomes thick slurry. The homogenate was then centrifuged at 4300 rpm for 5 minutes and the fat and supernatant layers were discarded. After centrifugation, the pellet was dissolved in 2.5mM SDC in PBS and incubated for 3 hours at room temperature on rotator. The solution was renewed and incubated for further 15 hours. Then, the remaining tissue was rinsed with water and washed PBS containing 1% P/S for 72 hours with solution change in each day [26].

G) **Delipidation, SDC, Triton X-100**: The tissue pieces were put in a beaker soaked in distilled water for 6 hours. Then, the following steps were done: 3% Triton X-100 in PBS for 12 hours, wash with distilled water containing 1% P/S for three times, 4% SDC for 24 hours, wash with distilled water containing 1% P/S for three times. Afterwards, the remaining tissue was lyophilized until the tissue became dried and treated with ethanol : dicholoromethane (Sigma, # 270997)(1:2 v/v) for 24 hours. The tissue was washed with sterile distilled water [70].

After applying each decellularization method, a small sample fragment of the decellularized tissue was stored for further histological and biochemical analysis and the remaining tissue pieces were collected in a falcon tube and stored at -80°C before lyophilization. Lyophilization was done until the tissue pieces were completely dried.

2.1.2 db-ECM solubilization and hydrogel formation

Lyophilized decellularized brain tissues were grinded with the addition of dry ice until becoming the powder form. Next, 1 mg/ml pepsin (Sigma, P6887) was dissolved in 0.1M hydrochloric acid (HCl, Sigma, # O7102) and different volumes of powdered db-ECM (10, 20 and 40 mg/ml) was added into the pepsin solution to became digested for 24 hours at room temperature on rotator. After digestion was completed, the digest solution was centrifuged at 13,000 rpm for 10 minutes and the solubilized db-ECM in the supernatant was reserved in a fresh Eppendorf tube. Solubilized db-ECM was neutralized on ice with cold 1M and 0.1M sodium hydroxide (Honeywell, #367176) and the pH was adjusted to 7.4 ± 0.2. 10X PBS (Biowest, #X0515) was added to the digest solution at the required amount. The formation of hydrogel was achieved incubating the neutralized solubilized db-ECM at 37°C for 45 minutes. For further applications, the neutralized digest solution was aliquoted in 250 µl and lyophilized for 48 h. The lyophilized powder was stored at -20°C until use. Before usage, the powder was resuspended in 250 µl

DMEM high glucose media containing 1% PSA and 50 µg/ml Fungin (Invivogen, #ant-fn-2).

2.2 Characterization of decellularized ECM

2.2.1 Measurement of the DNA content

The DNA content of brain ECM was quantified using Quant-iT PicoGreen dsDNA assay kit (Life Technologies Corporation, P7589). Native and decellularized wet tissues were sectioned into 5 mg samples. The samples were digested in 500 µl papain digestion buffer (pH=6.3), including 100mM EDTA, 100mM sodium phosphate,10mM L-cysteine HCl (Sigma, #30120) and 10mg/ml papain (Sigma, P4762) at 60°C for 21h. The samples were vortexed in every 4-5 hours. After incubation, the samples were lightly centrifuged and the supernatant was diluted 1:20 with 1X TE buffer. 100 µl diluted samples and dsDNA standards were transferred to a solid black 96-well plate. 100 µl picogreen solution was added to the each well. After incubation for 5 minutes in the dark at room temperature, the fluorescence was measured using a fluorescent plate reader with an excitation wavelength of 485 nm and emission wavelength of 520nm.

2.2.2 Measurement of Collagen content

The insoluble collagen content of native and decellularized brain was analysed using Sircol™ Collagen Assay (Biocolor, S2000), according to the manufacturer's instructions. Shortly, 20-30 mg of wet tissue was weighed and digested with Fragmentation reagent at 65 °C for 3 hours. Afterwards, samples were centrifuged at 12,000rpm for 10 minutes and the supernatant was diluted in a new tube. Sircol dye reagent was added and incubated for 30 minutes at room temperature. Then, centrifugation was done and the tubes were drained. Ice-cold acid -salt wash reagent was added and centrifuged again. The tubes were drained again and 1 ml alkali reagent was added to dissolve the pellets. The absorbance values of standards and samples at 550 nm were measured using a microplate reader (Bio-Tek Instruments, VT, USA). Absorbance values were normalized to sample weight.

2.2.3 Measurement of Sulphated Glycosaminoglycan (sGAG) Content

The sulphated glycosaminoglycan (sGAG) content of native and decellularized brain was quantified by using the Blyscan sGAG Assay Kit (Biocolor, B1000) following the

manufacturer's protocol. Briefly, 20 mg wet tissue samples were weighed and digested in papain extraction reagent containing 100 µg/ml papain at 65°C overnight. Blyscan dye reagent was added and the precipitated sGAG-dye complexes were dissolved with the dissociation reagent. The absorbance values of standards and samples at 656nm were measured using a microplate reader. Absorbance values were normalized to sample weight.

2.2.4 Brain Histology

Native and decellularized brain samples were fixed with 3.7% formaldehyde solution at 4 °C overnight. Fixed samples were embedded in OCT, frozen and 10 µm cryosections were mounted on glass slides. For DNA staining with Hoechst, slides were hydrated and stained for 15 minutes in 1 µg/ml Hoechst solution (Invitrogen) in PBS and visualized by fluorescence microscopy. For haematoxylin & eosin staining, slides were hydrated and stained with Mayer's haematoxylin (Abcam, ab128990) for 3 minutes followed by a 3-minute wash with tap water. Then, slides were immersed in 95% ethanol and stained with Eosin alcoholic solution for 45 seconds. For collagen staining, Sirius Red (PolySciences) in a saturated aqueous solution of picric acid was used. Slides were stained for one hour then rinsed in 0.5% acetic acid solution. Alcian blue staining was performed for sGAG assessment. Slides were hydrated and stained with 1% Alcian blue in 3% acetic acid solution pH 2.5 (Merck, #1.00063.2511) for 30 minutes followed by a 2-minute wash with tap water. After staining, all slides were dehydrated, mounted, coverslipped and visualized by light microscopy.

2.2.5 Mechanical analysis

Oscillatory rheology was performed using a Discovery HR-2 rheometer (TA instruments). 250 µl of the neutralized digested hydrogel sample was poured onto the lower plate which was precooled to 4 °C and 20 mm parallel plate was immediately lowered until the hydrogel fills the gap. Then, the lower plate was warmed to 37°C, storage and loss moduli were measured for 30 minutes with a fixed frequency of 0.5 Hz and 0.1% strain. When storage moduli of the sample reached an equilibrium state, a creep-recovery test was performed where 0.1 Pa shear stress was applied for 15 minutes and strain was measured, then sample was unloaded, and strain was recorded over time. All measurements were done in triplicate.

2.3 Cytocompatibility of db-ECM

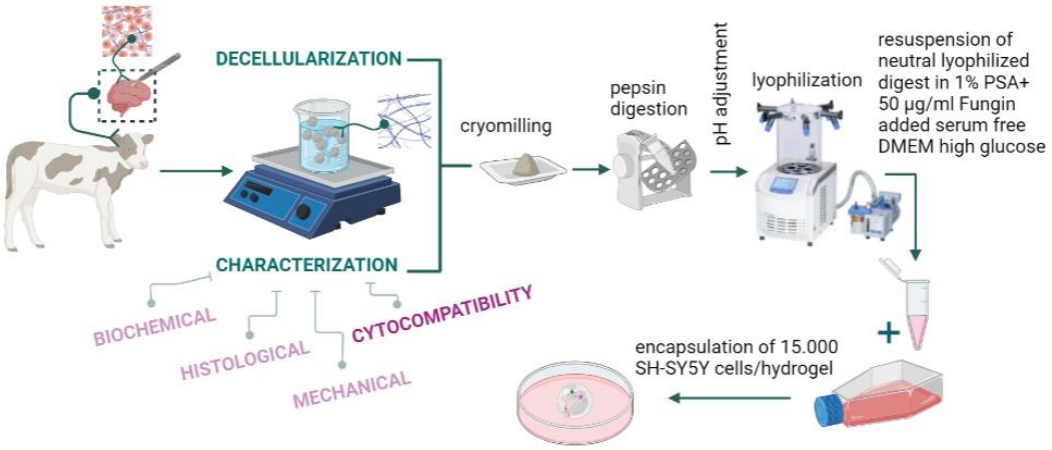

Figure 4 Experimental scheme for encapsulation of neuroblastoma cells in the hydrogels (Created with BioRender.com).

2.3.1 Cell line and cell culture

The human neuroblastoma cell line, SH-SY5Y, (ATCC, CRL-2266™) was cultured in Dulbecco's Modified Eagle Medium with 4.5g/L D-glucose (DMEM)(Sigma, RNBK3727) containing 10% heat-inactivated Fetal Bovine Serum (FBS, Biowest, # S181H-500) and 1% P/S. Cells were incubated at 37 °C in a humidified atmosphere with 5% CO_2. The media was changed every other day and the cells were passaged when they reach enough confluency (~80%). Cells were used to evaluate the cytocompatibility and 3D cell encapsulation ability of the hydrogels derived from db-ECM as shown in the *Figure* 4.

2.3.2 Cell encapsulation in the db-ECM pregel

Neutralized db-ECM digest powders were stored at -20°C until cell encapsulation. The db-ECM digests powder was resuspended in DMEM high glucose medium containing 1% PSA and 50 µg/ml Fungin. The cells were embedded in the db-ECM digests at a concentration of $5x10^5$cells/ml and after mixing the cells with db-ECM digests, 3D hydrogels were created on the 24-well plate. The plate was incubated at 37°C for 1 hour to allow gelation, and 1 ml complete cell culture medium was added onto cell-laden hydrogels carefully. The culture medium was renewed every 3 days.

2.3.3 Cell viability assay (CTG 3D assay)

The cell-laden hydrogels were prepared using db-ECM digests and SH-SY5Y cells. On days 1, 4, and 9 CellTiter-Glo 3D assay (Promega) was performed. For this purpose, CTG-3D assay reagent with fresh cell culture medium was added into each well on the depicted time points. After shaking and incubation for 45 minutes, the cell culture medium was transferred to the black-wall 96-well plate to measure the luminescence using microplate reader. A growth curve was created for selected db-ECM hydrogels.

2.3.4 Immunostaining

SH-SY5Y cells were encapsulated in decellularized brain hydrogels with a concentration of 15.000 cells/hydrogel and were fixed with 4% paraformaldehyde (Sigma, 158127-500G) after 4 days in culture. For permeabilization, 0.1% Triton X-100 in PBS was treated for 1 hour at room temperature. Then, blocking was done with 1% Bovine Serum Albumin (Sigma, A2153-10G) solution including 10% goat serum for 2 hours. Primary antibodies anti-Neun (Abcam, ab177487) and anti-Beta-Tubulin III (Biolegend, #801213) were used for immunolabelling. After overnight incubation at 4°C in constant rotation, secondary antibodies Goat Anti-Mouse IgG (H+L), FITC conjugated (Jackson Immunoresearch, #115-095-003) and Goat Anti-rabbit, Alexa Fluor 594 (Invitrogen, R37117) were treated in dark. Nuclear counter staining was done with 4′,6-diamidino-2-phenylindole (DAPI, Sigma, # MBD0015-10 ML) and images were taken with confocal microscopy. After blocking, another sample set was stained with Phalloidin-iFluor 488 Reagent (Abcam, ab176753) and DAPI. Similarly, the images were taken with Leica DMI/SP8 laser scanning confocal microscope. Image analysis was done using ImageJ software (National Institutes of Health, USA).

2.4 Neuronal Differentiation

2.4.1 2D neuronal differentiation

The human neuroblastoma cell line, SH-SY5Y, (ATCC, CRL-2266™) was cultured in DMEM with 4.5g/L glucose containing 10% heat-inactivated FBS and 1% P/S. Cells were incubated at 37 °C in a humidified atmosphere with 5% CO_2. The media was changed every other day and the cells were passaged when they reach enough confluency (~80%). Cells at passage number 17-20 were used to evaluate the differentiation ability

of the cells in 2D and 3D environments. The cells were seeded into the 6-well plate at a cell density of 30.000 cells/well. As shown in *Figure* 5, FBS content was gradually decreased until 2.5 µM and 10 µM RA with 2mM L-Glutamine was added to the DMEM high glucose medium. After reaching day 9, the differentiation medium was switched to the neurobasal medium (GibCo, #A35829-01) containing 2.5% FBS, 1% P/S, 10 µM RA (Sigma, #R2625-50MG), 2mM L-Glutamine (Biowest, #X0550-100), 1X N-2 (Gibco, #17502), 1X B-27 Plus supplement (Gibco, #A35828-01) and 20mM Potassium Chloride (KCl, Sigma, P9333).

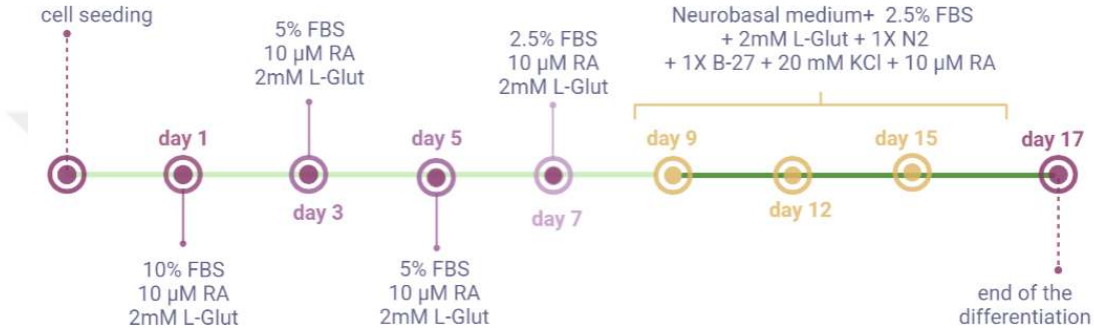

Figure 5 Neuronal differentiation treatment timeline for 2D and 3D application (Created with BioRender.com).

2.4.2 3D neuronal differentiation

Neuroblastoma cells cultured and expanded on 2D were encapsulated into db-ECM hydrogels at a cell density of 1.6 x 10^5 cells/ml. For this purpose, the lyophilized db-ECM digest was thawed in 200 µl DMEM high glucose medium with 1% PSA and 50 µg/ml Fungin. 4x10^4 cells were resuspended in 50µl complete DMEM high glucose medium and mixed well with the db-ECM by pipetting. Immediately, the cell encapsulated db-ECM was plated in 30 µl droplets in 24-well suspension plate. The generated hydrogels were incubated at 37°C for 45 minutes to allow gelation. Then, 600 µl complete DMEM high glucose medium was put from the side of the plate into each well without disrupting the hydrogels.

The exact differentiation timeline indicated in *Figure* 5 was applied to the 3D culture as well. At the end of the differentiation procedure, the hydrogels were either collected by micro spoon for the extraction of RNA or fixed with 4% PFA for immunostaining.

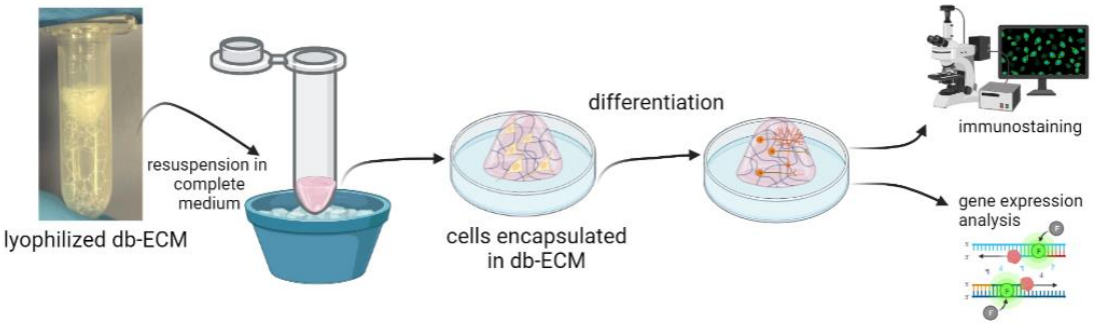

Figure 6 Experimental design for 3D differentiation (Created with BioRender.com).

2.4.3 RNA isolation and c-DNA synthesis

RNA extraction from 2D cultured cells were applied following the manufacturer's instructions lead by MN™ NucleoSpin-RNA isolation kit (Macherey-Nagel, #2111/002). For 3D cultured cells, RNA extraction was done according to the NucleoSpin®-RNA support protocol for difficult-to-lyse tissue (Rev.02). Briefly, 3D-differentiated cells encapsulated gels were collected in an Eppendorf tube and stored at -80°C until it was completely frozen. Then, the gels were homogenized by pestle in the RA1 buffer supplemented. After incubation on ice, the homogenized gels were centrifuged at 14000 g for 5 minutes to remove the debris. Same amount of absolute ethanol was added to the supernatant and mixed well by vortexing following with centrifugation at 14000 g for 10 minutes at 4 °C. Supernatant was discarded and the pellet was air-dried. After resuspension of the pellet, the instructions were followed accordingly which includes RNA binding, membrane desalting, DNA digestion, purification, and elution. The quantity and quality of the eluted RNA was evaluated with NanoDrop Spectrophotometer (Thermo Scientific 2000c, USA).

The purified RNA was then reverse transcribed into cDNA and for this purpose 1 µg RNA was used. In the first step of the synthesis random hexamer, 1 µg RNA, 10mM dNTPmix, and distilled water was mixed. After incubation at 65°C for 5 minutes, the second mixture including 5x First strand buffer, 100mM DTT, Ribonuclease Inhibitor (40 Units/µl) was added to each sample. The incubation was done at 37°C for 2 minutes and M-MLV RT (200 units). The incubation for synthesis was achieved as such: 25°C for 10 minutes, 37°C for 50 minutes and 70°C for 15 minutes. The synthesized cDNA was then diluted 1:5.

2.4.4 Gene expression analysis

Neuronal development related gene expressions were quantified relatively by RT-q-PCR. The primers were designed using Primer ™ software and purchased from Sentebiolab. The gene-specific primer sequences are as shown below in *Table* 1.

Table 1 Gene specific primers used in RT-PCR.

Gene	Forward primer (5'→3')	Reverse primer (5'→3')
APP	ATGGTAATGCTGGCCTGCTG	GAATCCCACTTCCCATTCTG
CHAT	GAGGAGCAGTTCAGGAAGAG	CCAGGAGTTTCTGCTGCAGG
GAPDH	CTGACTTCAACAGCGACACC	GTGGTCCAGGGGTCTTACTC
GFAP	CCAGTTATCAGGAGGCGCTG	TCCTGGTACTCCTGCAAGTG
MAP2	CTGTAGCAGTCCTGAAAGGTG	CTGTTCTGAGGCAGGTGATG
MAPT	TTAGCAACGTCCAGTCCAAG	TCAGGTCAACTGGTTTGTAG
PSEN1	AGTATCCTCGCTGGTGAAGAC	ACGAAACAGGCTATGGTTGTG
RET	ACCATGGGCGACCTCATCTC	CTGCCAAGTCCCGATGAACG
SOX2	CTTTTATGAGAGAGATCCTG	ACCGTACCACTAGAACTTT
SYP	GCTGTGTTCGCCTTCATGTG	AATGTTCTCTGGGTCTGTGG
TUBB3	GAGCGGATCAGCGTCTACTAC	GCGGACACTGTCCATGGTTC

5µl 2x QuantiNova SYBR Green PCR Master Mix (Qiagen, #172034345), 1 µl forward and reverse primers, 1 µl cDNA template and 1 µl PCR grade water was mixed for the reaction of each experimental group and transferred to the PCR plate. Reaction cycles were carried out by Roche's LightCycler 480 Instrument II.

Table 2 Reaction conditions for RT-q-PCR.

STEP	Initial denaturation	Denaturation	Annealing	Elongation	Melting curve			*Cooling*
°C	95°C	95°C	56°C	72°C	95°C	65°C	97°C	*40°C*
Time	5 min	30 s	30 s	30 s	10 s	1 min		*30 s*
Cycle #	1	40			1			*1*

The mRNA expression levels (depicted as Cq values) of the related genes were normalized to a housekeeping control gene which is GAPDH, and the fold change was calculated using the $2^{-\Delta\Delta Ct}$ method.

2.4.5 Immunostaining with neuronal markers

SH-SY5Y cells encapsulated in db-ECM hydrogels with the concentration of 15.000 cells/hydrogel and 2D cultured cells for both undifferentiated control and differentiated group were fixed with 4% paraformaldehyde (Sigma, 158127-500G) at day 15. For permeabilization, 0.1% Triton X-100 in PBS was treated for 1 hour at room temperature for 3D culture and 15 minutes for 2D culture. Then, blocking was done with 1% Bovine Serum Albumin (Sigma, A2153-10G) solution including 22.52 mg/ml glycine in PBS-T for 2 hours for 3D culture and for 30 minutes for 2D culture. Primary antibodies anti-Neun (Abcam, ab177487) and anti-Beta-Tubulin III (Biolegend, #801213) were used for immunostaining. After overnight incubation at 4°C in constant rotation, secondary antibodies Alexa Fluor 488 goat anti-mouse IgG (H+L) (Invitrogen, A11029) and Alexa Fluor 594 goat anti-rabbit (Invitrogen, R37117) were treated in dark. Nuclear counter staining was done with 4′,6-diamidino-2-phenylindole (DAPI, Sigma, # MBD0015-10 ML) and images were taken with Leica DMI/SP8 laser scanning confocal microscope. Image analysis was done using ImageJ software (National Institutes of Health, USA).

2.5 Statistical analysis

The stated quantitative data with mean ± S.D values were performed minimum n=3 triplicates. One-way analysis of variance (ANOVA) with Tukey post-hoc tests were applied to all experimental data using GraphPad Prism 8 software. P values of <0.05 were considered statistically significant. Prism's recommended classification for significance was followed ($p < 0.0001$ = extremely significant (****), $0.0001 < p < 0.001$ = extremely significant (***), $0.001 < p < 0.01$ = very significant (**), and $0.01 < p < 0.05$ = significant (*)).

Chapter 3: **RESULTS**

3.1 Fabrication of decellularized brain tissues and confirmation of nuclear content elimination

Bovine brain tissue was decellularized and were further processed with the following steps: lyophilization, cryo-milling, and digestion. After solubilizing the db-ECM through digestion with the pepsin enzyme on rotator for 24 hours, neutralization to physiological pH was performed to generate db-ECM hydrogels via thermal crosslinking (*Figure* 7). Validation of decellularization, in which confirmation of nuclear elimination was done, was achieved after decellularization using the wet tissues. Along with nuclear content evaluation, histological examination, and biological content analysis, including sGAG (sulphated glycosaminoglycans) and collagen content, were also done. At the stage of hydrogel construction, biomechanical characterization was achieved using oscillatory rheometer. Cells adaptation with the created hydrogels were reviewed after encapsulation of neuroblastoma cells. As shown in the *Figure* 8a, physical, chemical, biological and different combinations of these methods were applied for decellularization of bovine brain tissue.

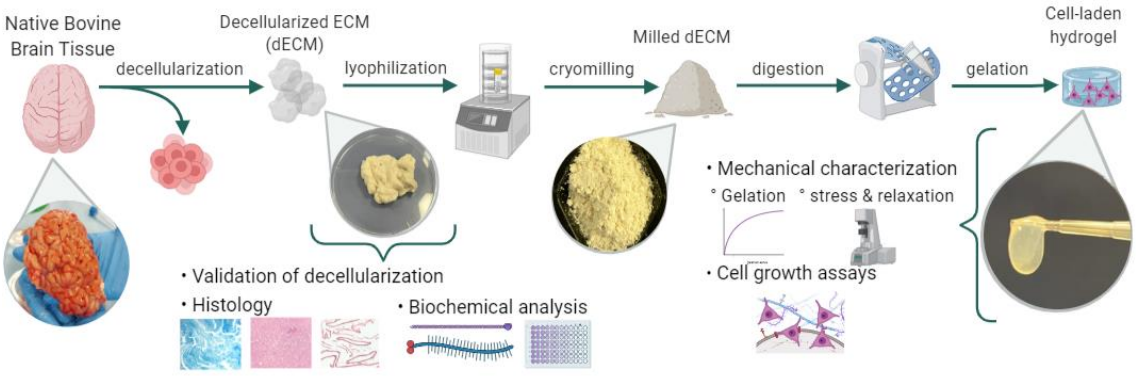

Figure 7 Pipeline for generation of hydrogel from native bovine brain (Created with BioRender.com).

As indicated in the *Figure* 8b, the morphological properties of options D, E and G were distinctive when compared with other decellularization options, while others were had resemblance to the native tissue. Notably, the cytoplasm and extracellular matrix stained

by Eosin dye have fiber-like structures within the remaining tissue after applying decellularization methods D,E, and G.

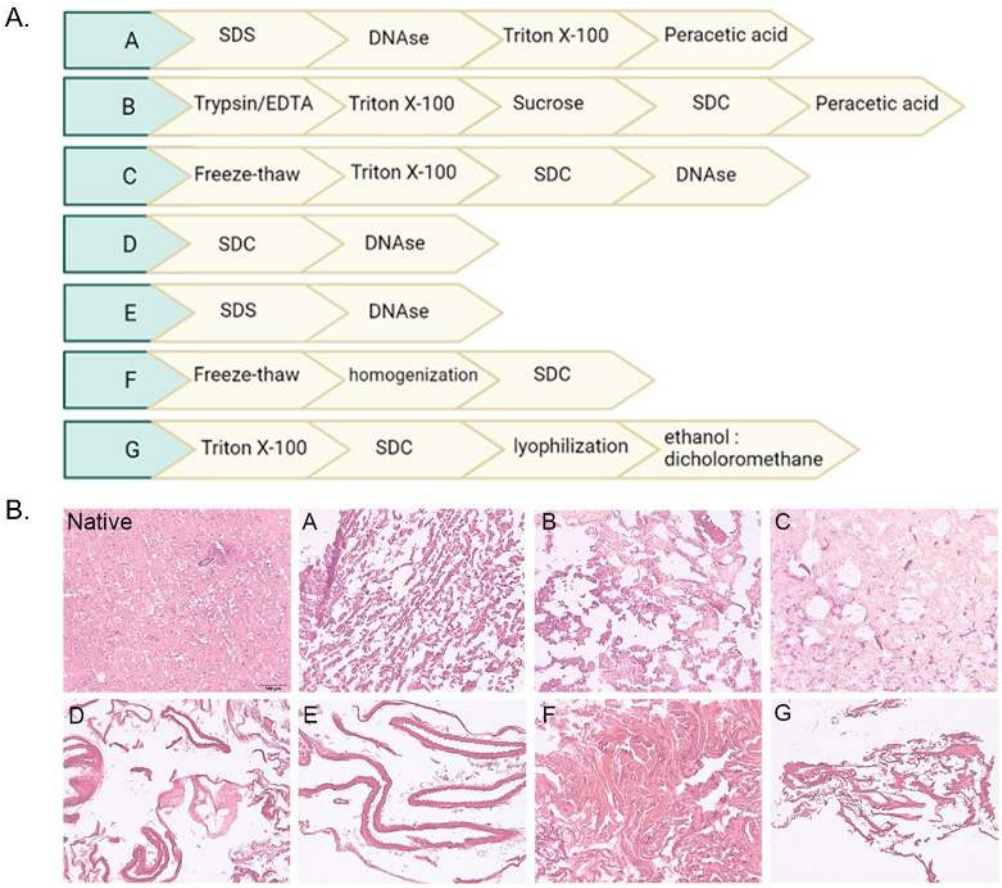

Figure 8 Decellularization methods applied. a) Scope of different decellularization methods (Created with BioRender.com) b) Histological examination with H&E staining (scale bar: 100µm).

First of all, the efficiency of the decellularization processes was confirmed by the evaluation of the DNA content and PicoGreen assay was used for this purpose. As shown in the *Figure* 9a, the DNA content was significantly reduced in each decellularized sample when compared with the native brain tissue, but especially several methods were more effective: 20.25±9 ng DNA per mg wet tissue in option C, 3.45±5 ng DNA per mg wet tissue in option D, 62.01±20 ng/mg wet tissue in option E and 59.16 ng/mg wet tissue in option G vs. 380 ± 49 ng DNA/wet tissue in native tissue. These results were also confirmed qualitatively with H&E and Hoechst staining. More clearly, Hoechst staining shows remaining nuclei in options A and B, whereas other options were successful at DNA elimination (*Figure* 9b).

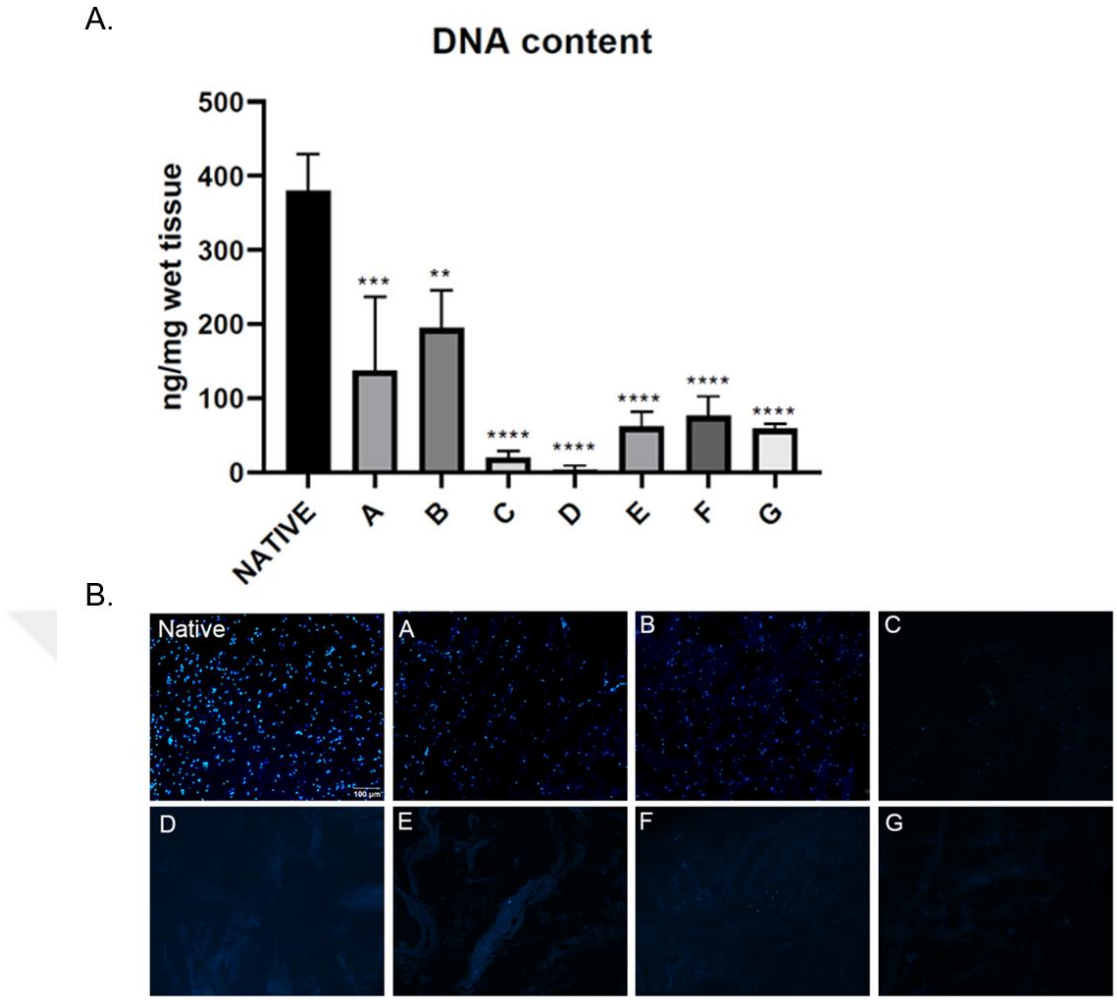

Figure 9 Confirmation of decellularization. a) Quantification of double stranded DNA b) Hoechst staining of native and decellularized tissues (scale bar: 100μm).

3.2 Biochemical characterization of decellularized tissues

After decellularization was confirmed by showing nuclear content elimination, the biochemical composition of the decellularized tissues was analyzed. As shown in *Figure* 10, collagen and sGAG were both quantitatively and qualitatively examined. In options D, E, F, and G, there observed an extreme increase in the insoluble collagen content whereas, in the options A, B, and C remained unchanged (F*igure* 10b). This increase was also confirmed by Sirius red staining, as dense collagen fibers were explicitly shown (*Figure* 10a). On the other hand, according to the quantitative assay based on 1,9-dimethylmethylene blue dye, it was concluded that sGAG levels were retained in options A, B and G. Treatments in other decellularization methods (C, D, E, F) caused a decrease in sGAG content in decellularized tissues (*Figure* 10d). This remarkable decrease in

sGAG content in the samples with C, D, E, and F decellularization options were also validated with Alcian blue staining (*Fig*ure 10b). Briefly, various decellularization agents have different effects on the preservation of ECM components and the methods D,E,F, and G cause a significant increase in the collagen content.

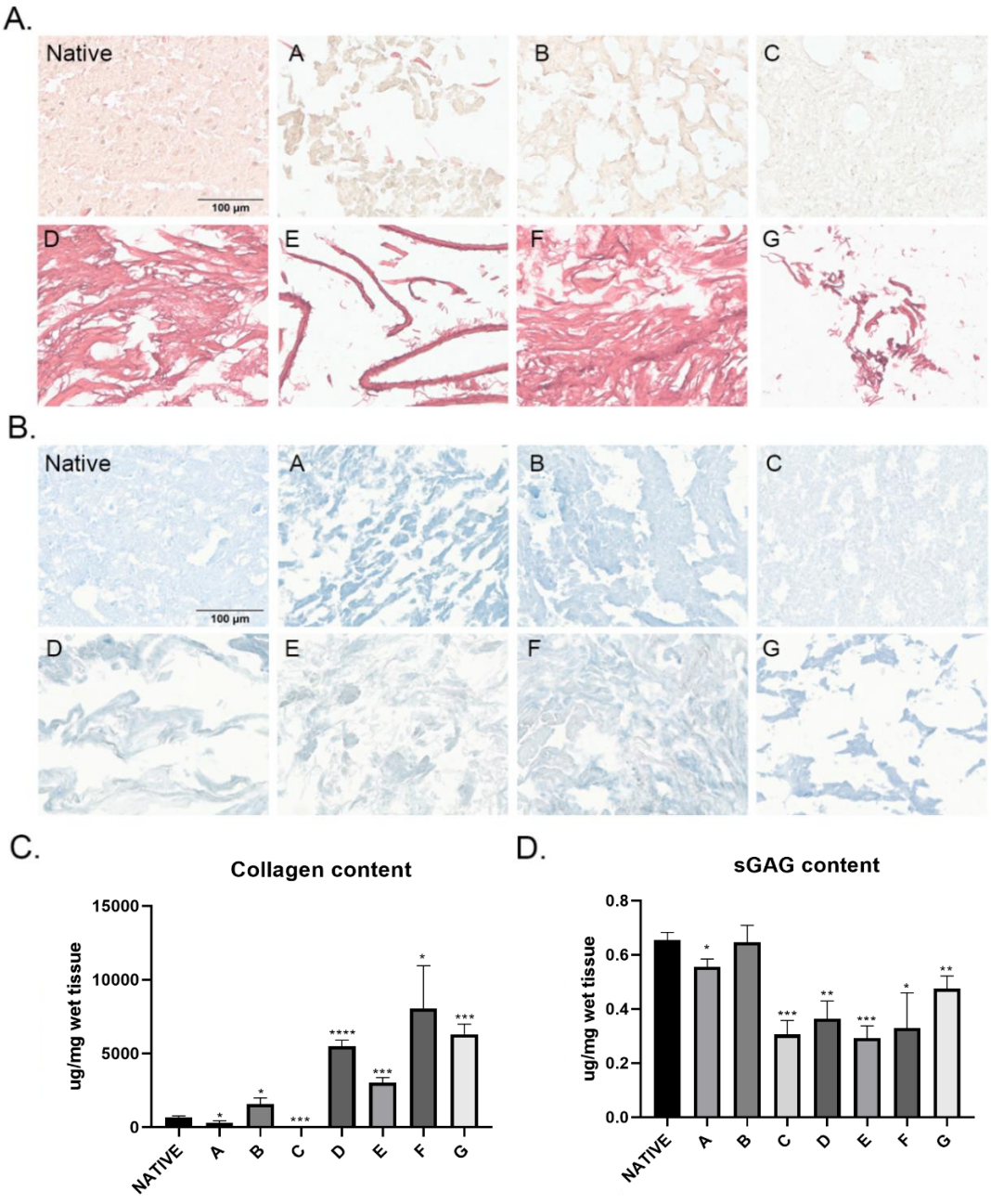

Figure 10 Evaluation of ECM protein retention: a) Indication of collagen content by Sirius red staining b) sGAGs by Alcian blue staining (scale bar: 100µm) c) Quantification of insoluble collagen contents d) Quantification of sGAG contents.

3.3 Gelation trials of hydrogels

ECM derived from decellularized bovine brain tissue was used to fabricate hydrogels. Further processing of db-ECM led several options to solidify whereas others to fail during the hydrogel formation. After decellularization, the tissues were lyophilized until became completely dry and then cryo-milled. Subsequently, the powdered tissues were digested with pepsin in an acidic milieu for 24 hours with constant rotation. In *Figure* 10, 'pre-gel digest' images are showing acidic forms of digests after 24 hours of incubation. Although powder was solubilized to a large extent during digestion, in order to get rid of the remaining insolubilized powder traces, the digest was centrifuged and only the soluble part was further processed. It was observed that the total content of the digests led to heterogeneous gel formation. Then, soluble digests were neutralized with sodium-hydroxide, and pH was arranged to the physiological state, i.e., 7.4. After incubating the neutralized digests at 37°C, options D, E, F and G showed successful gel forms whereas A, B, and C failed (*Figure* 11). Several treatment options, E with SDS and G with delipidation, were able to form gels at different concentrations (10 mg/ml and 20 mg/ml powder). It was also figured out that the opacity, characteristic of gels, elasticity, and durability varies with the concentration of the powdered db-ECM in digests and the treatments in decellularization. Further mechanical analyses were done as shown below.

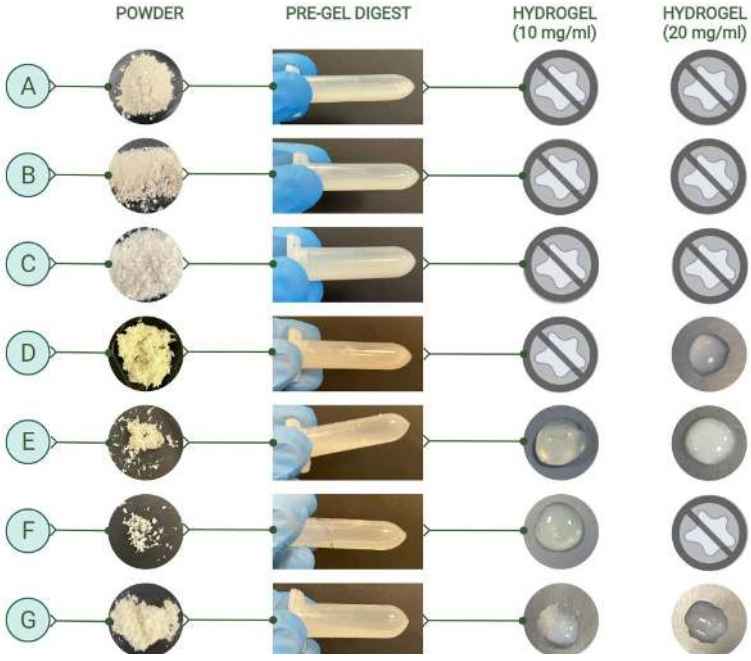

Figure 11 Representation of gelation results: powder after cryomilling, pre-gel digest forms before neutralization, hydrogel formation at 37°C after neutralization. (Created with BioRender.com).

3.4 Gelation kinetics analysis for db-ECM hydrogels

Mechanical properties of db-ECM hydrogels that were able to form a gel-like structure were assessed by oscillatory rheology. Pre-gels obtained by decellularization methods D (20 mg/ml), G (10 mg/ml and 20 mg/ml), E (10 mg/ml) and F (10 mg/ml) were able to form hydrogels in 10 minutes during the temperature ramp and exhibited complete gelation in all trials (*Figure* 12a). Furthermore, the storage modulus of hydrogel samples was higher than the loss modulus, again indicating the gelation capabilities of the db-ECM hydrogels (*Figure* 12c, d). Even though there was a non-significant difference in stiffness of the hydrogels obtained by decellularization methods, we observed that sample G20 and F were mechanically more stable than others while stability of sample D, G10 and E were similar. Interestingly, permanent strain preserved on the hydrogels after creep test, which indicates the viscoelastic properties of hydrogels, were significantly different in samples D and E that have similar G' values (*F*igure 12e). Moreover, G20 and F hydrogels with similar rigidities exhibited different viscoelastic properties. However, creep-recovery test was not achieved on sample G10 since the gel-like structure was destroyed during the creep application. Briefly, these results demonstrated that decellularization techniques determine the mechanical properties of decellularized bovine brain derived hydrogels.

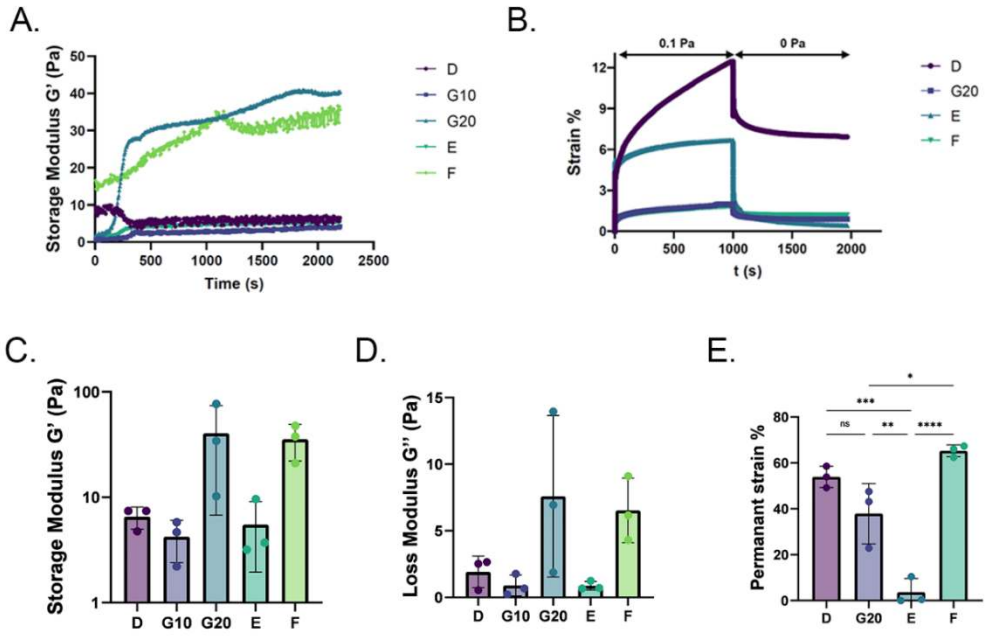

Figure 12 Gelation kinetics analysis for db-ECM hydrogels. a) Storage modulus of hydrogels with indicated concentrations. b) Creep-Recovery analysis. c) Final storage modulus for selected gelling hydrogels. d) Final loss modulus for selected gelling hydrogels. e) Permanent strain % of selected gelling hydrogels after recovery.

3.5 Cytocompatibility properties of hydrogels

The cytocompatibility was assessed by encapsulating human neuroblastoma cells in 3D hydrogels. For this purpose, only gelling hydrogels were considered and CellTiter-Glo® Luminescent Cell Viability Assay was applied to quantify the viable cells (*Figure* 13). After day 1, the viable cells were present in each method which provide confirmation of the detergent-free milieu. In comparison to other methods, option D showed the least cell proliferation. A linear proliferation was observed until day 9.

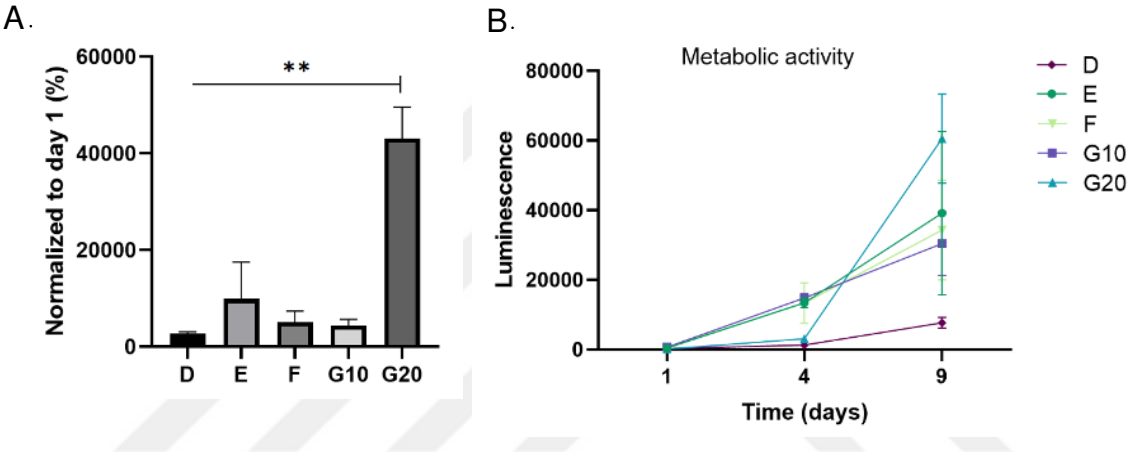

Figure 13 Metabolic activity of neuroblastoma cells encapsulated in hydrogels. *a)* Metabolic activity assay in 3D cell-laden hydrogels, data normalized to day1, b) metabolic activity screen for 9 days.

Starting from day 4, the gels became contracted and the size of the hydrogels became smaller. The cells tend to form clusters and reshape the gels. Contraction of the gel remarkably occurred in option F, so the cluster of cells became densely populated within the hydrogel as shown in *Figure* 14a. On day 4th, neurite formation was started to be observed in options E, G10, and G20. In option D, the cells could not form cell clusters and there was a decrease in cell density. As indicated by immunocytochemical staining, there was evenly distributed cell clusters in option E and G10. Cluster formation was not regularly organized by option G20. Finally, methods E and G10 outperformed the other gelling methods in terms of neuronal cytocompatibility and viability.

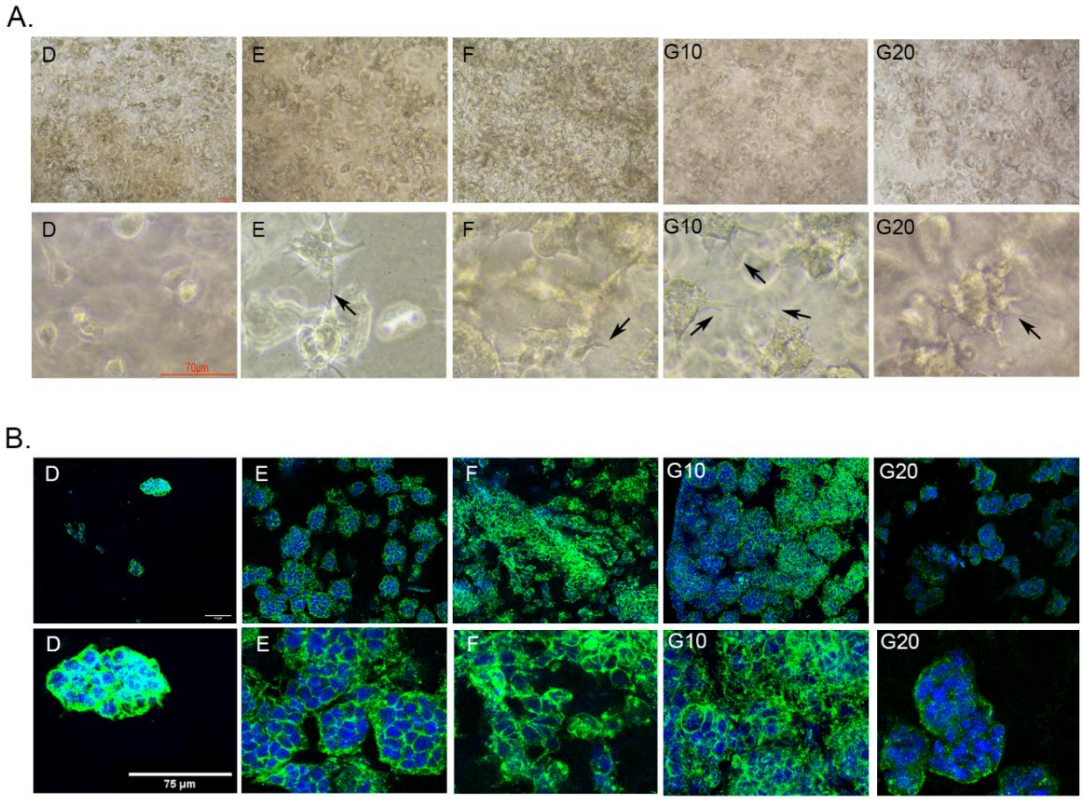

Figure 14 Images of encapsulated neuroblastoma cells. a) Brightfield images of 3D neuroblastoma cell-laden hydrogels, 15.000 cells/hydrogel at day 4. Scale: 100µm (top panel) and 70 µm (bottom panel). b) Immunocytochemical staining images of 3D neuroblastoma cell-laden hydrogels, 15.000 cells/hydrogel at day4. green: phalloidin, nuclear staining (DAPI: blue). Scale: 75 µm (top and bottom panel).

3.6 Immunostaining of neuroblastoma cells encapsulated in hydrogels

Further immunocytochemical studies were performed in order to verify the presence of neuronal markers in 3D db-ECM hydrogels. For this purpose, NEUN, as a neuronal nuclei marker, and TUBB3 (class III β-tubulin), as a mature neuron marker, were investigated in neuron cultures embedded in hydrogels. As shown in the *Fig*ure 15, neurons cultured in options D, E, F, and G hydrogels were positive for the selected neuronal markers, indicating that bovine brain derived decellularized hydrogels can recapitulate the native brain ECM environment to sustain human neural cells.

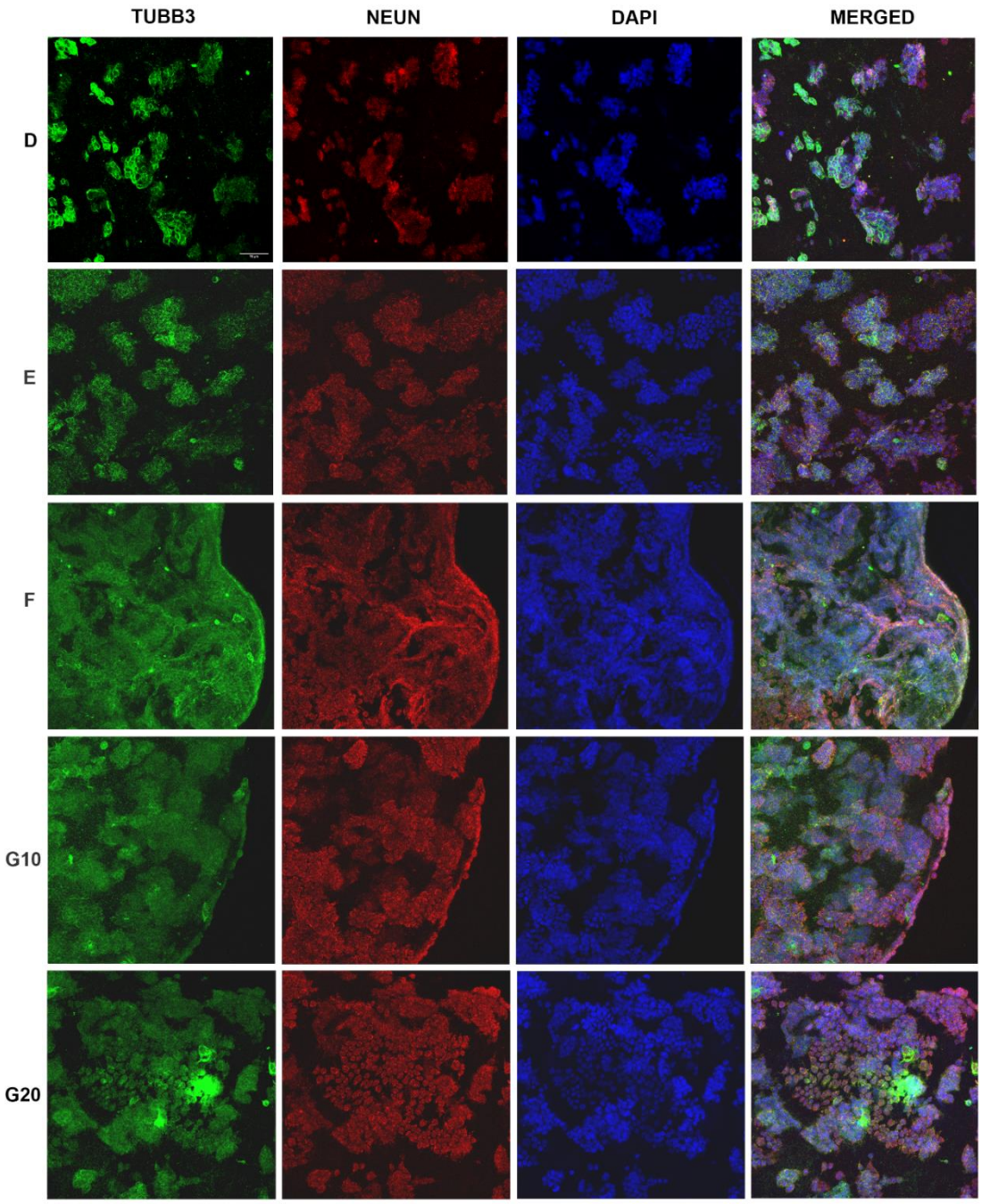

Figure 15 Immunocytochemical staining images of 3D neuroblastoma cell-laden hydrogels, 15.000 cells/hydrogel at 4th day. Neuronal markers: Beta-tubulin III: green, Neun: red, nuclear staining (DAPI: blue) (scale bar: 75 μm).

3.7 Differentiation of neuroblastoma cells in 3D hydrogel

Differentiation protocol was performed to the neuroblastoma cells for 17 days and the procedure included two differentiation phases. In the first phase, the content of the serum was gradually decreased within the DMEM high glucose medium containing RA, while, in the second phase, the cells were fed with neurobasal medium containing various neurotrophic factors. The morphology of the cells was carefully controlled under brightfield microscopy during the differentiation protocol optimization trials. The brightfield images taken at the end of the trial, at day 17, were shown below in *Figure* 16. The differentiated cell population was decreased in number in comparison to the control group in both 2D and 3D conditions. Apart from reduced cell proliferation, the morphology of the cells was remarkably changed in the 2D and 3D conditions. In 2D platform, differentiated cells displayed elongated axons creating synaptic network, while the cell body became smaller in size. In 3D culture, the encapsulated naïve cells in the control group were inclined to form round cell clump masses. On the other hand, the differentiated cells were tended to form neurites towards nearby cells across the hydrogel without forming cell clusters.

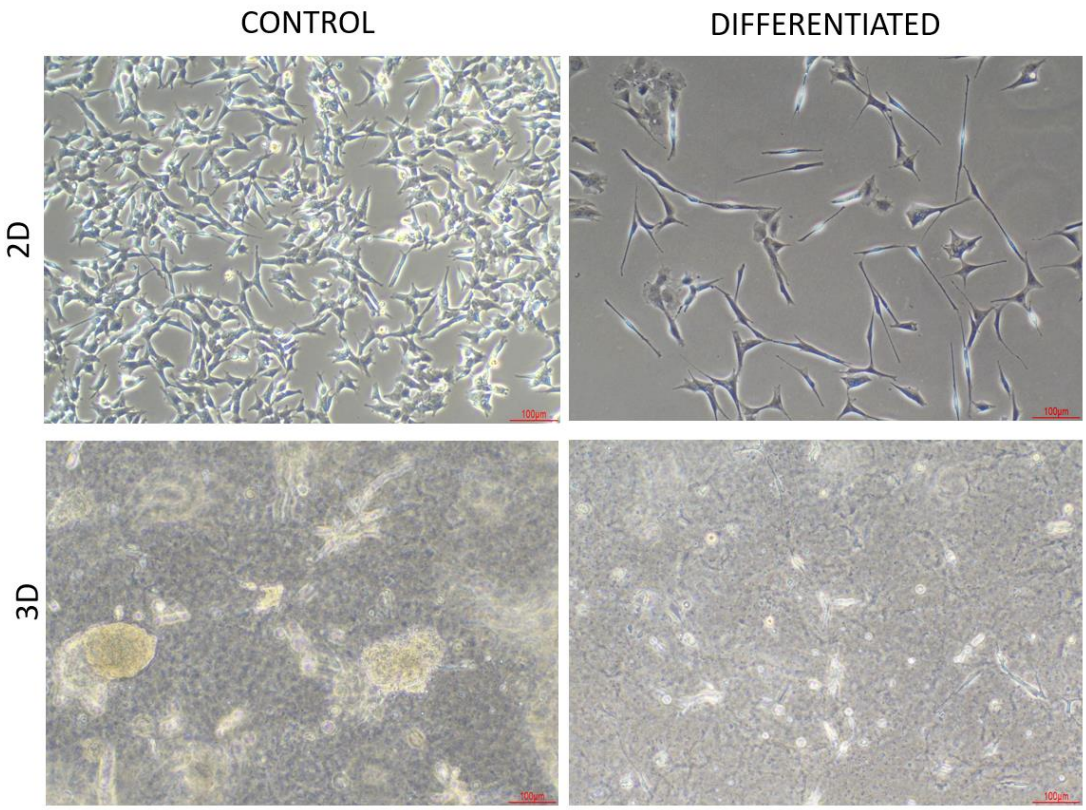

Figure 16 Brightfield images of undifferentiated and differentiated neuroblastoma cells in 2D and 3D microenvironment (scale bar: 100µm).

3.8 Gene expression analysis of the differentiated cells

Since gene expression profile is crucial for the cellular fate during differentiation, gene expression levels were relatively quantified by RT-q-PCR (*Figure* 17). For this purpose, cells were grown in 2D and 3D conditions and RNA was extracted from the cells at the end-point of the differentiation. Then, mRNA was converted into cDNA to be used in RT-q-PCR. *GAPDH* was used as an internal control and the expression levels of the selected genes, which were possibly related with neuronal differentiation, were quantified. *TUBB3*, a mature neuron marker, is increased much more in 2D culture than 3D culture. However, in both conditions, an increase in the gene expression was observed for *TUBB3* marker. Another investigated marker as a cholinergic neuron marker, *CHAT* was also significantly increased in both conditions. Unexpectedly, *MAP2*, a responsible gene for neurogenesis, was decreased in gene expression in both conditions. In 3D cultured cells, this decreased was observed more strikingly. Although there were some correlations in gene expression profiles, there were also some exceptional markers which were differently affected after the applied differentiation procedure. *SOX2*, a stemness marker, was significantly decreased in gene expression in 2D cultured differentiated neuroblastoma cells in comparison to control group. However, not any significant alteration was observed by 3D cultured cells. Similarly, reduced levels of *MAPT* gene expression were observed by 2D cultured differentiated cells, while no difference was recorded for 3D cultured cells. Another marker related to the neuronal differentiation, in which changes was shown, was *RET* and an increase was observed as 2.64-fold in the 2D cultured differentiated cells in comparison to control group. In 2D-cultured experimental groups, there was not any significant changes in gene expression levels of the following genes: *APP*, *PSEN1*, *GFAP*, *SYP*. Apart from the above indicated alterations, several genes were differentially expressed in 3D encapsulated cells only. *GFAP* (2.78-fold) and *SYP* (1.59-fold) gene expressions were remarkably elevated in 3D cultured differentiated cells.

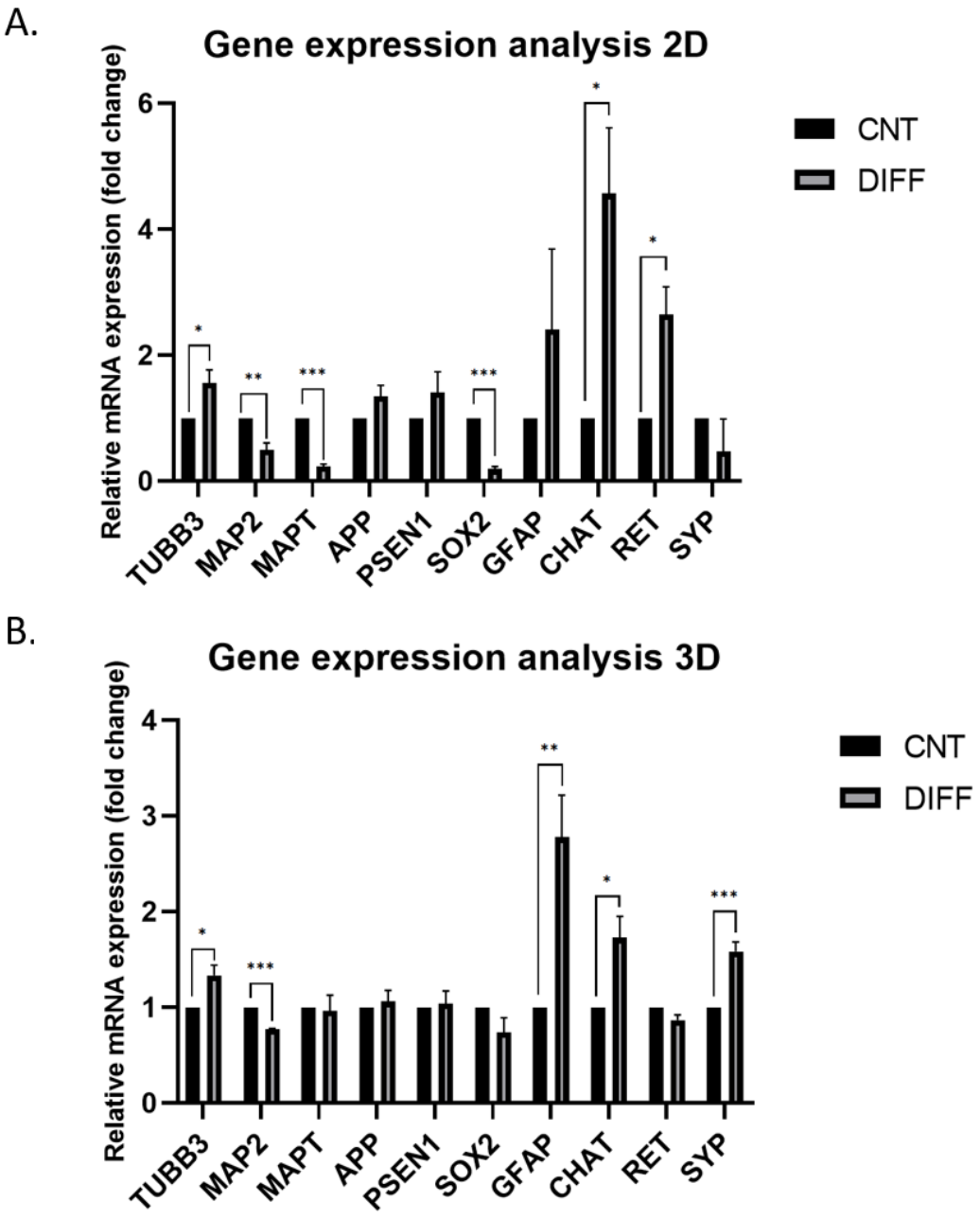

Figure 17 Gene expression analysis of 2D differentiated cells (a) and 3D differentiated cells (b), the results were normalized to GAPDH expression of the cells.

3.9 Evaluation of neuronal markers with immunostaining in differentiated cells

In order to evaluate the structural changes in differentiated cells in 2D and 3D cultures, immunostaining with neuronal nuclei marker NEUN, mature neuron marker beta-tubulin III (TUBB3) and nuclear counter-stain DAPI was applied. As shown in *Figure* 18, the number of cells in the differentiation group was reduced distinguishably in the 2D culture. The present cells have elongated axons expressing TUBB3 protein. The nuclei of the mature neurons are more in linear form than the control cells.

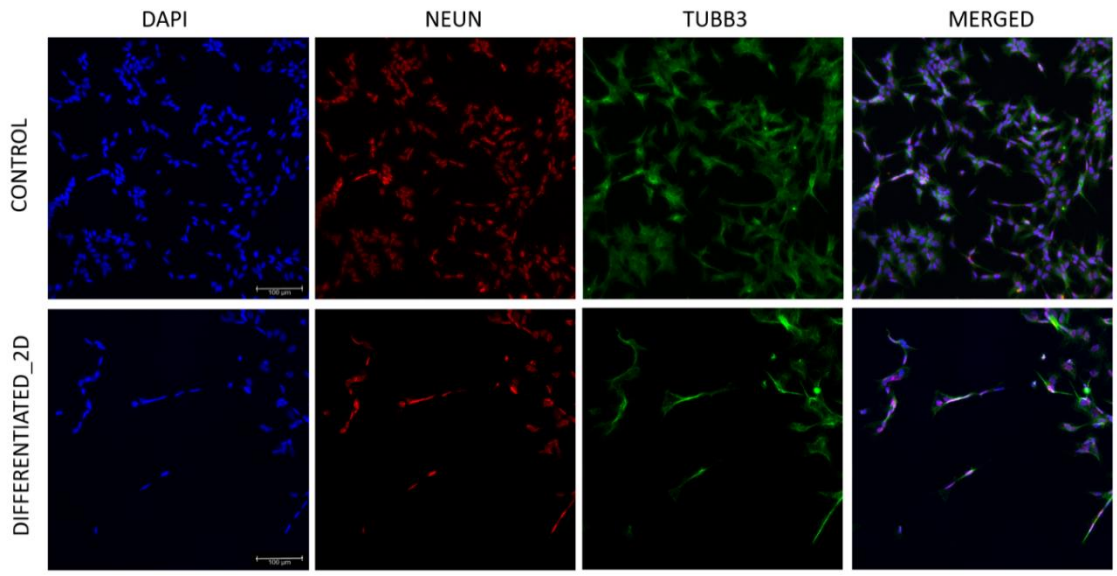

Figure 18 Immunostaining of undifferentiated and differentiated neuroblastoma cells in 2D culture at day 15; Neuronal markers: Beta-tubulin III: green, Neun: red, nuclear staining (DAPI: blue) (scale bar: 100 µm).

To examine the effect of the 3D ECM within the culture, the neuroblastoma cells were encapsulated in the hydrogel which was derived from decellularized bovine brain tissue. The differentiation protocol, which was described previously, was applied accordingly and the cells were fixed to be proceeded for immunostaining. In the control group, cell clump formation was observed. The cells forming the clusters had small neuronal projections without forming neuronal synaptic network. However, the differentiated cells in the 3D culture formed network with the surrounding cells and these cells were expressing TUBB3 progressively (*Figure* 19).

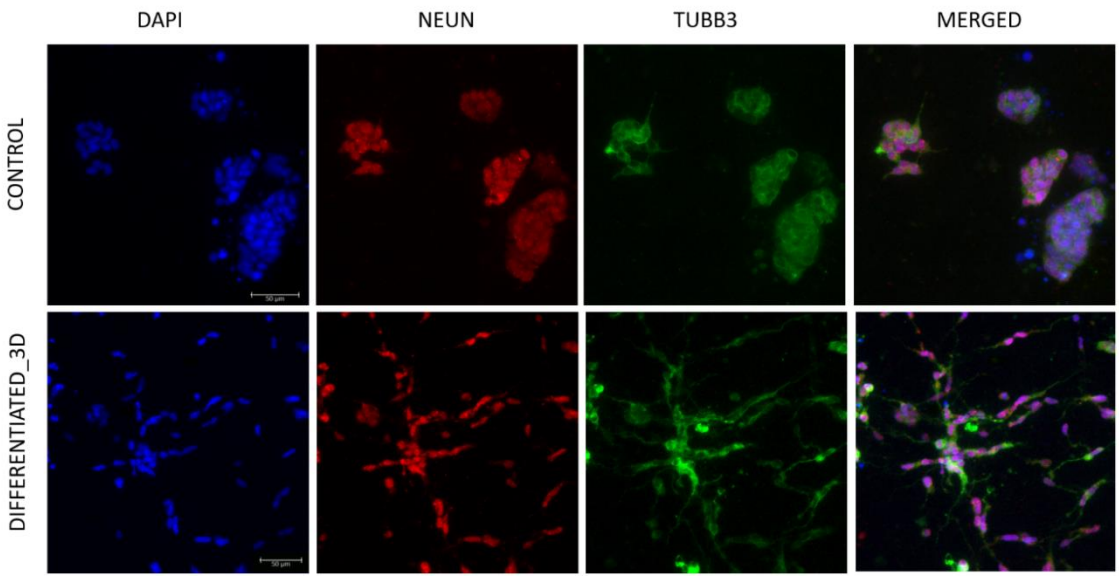

Figure 19 Immunostaining of undifferentiated and differentiated neuroblastoma cells in 3D culture at day 15; Neuronal markers: Beta-tubulin III: green, Neun: red, nuclear staining (DAPI: blue) (scale bar: 100 µm).

Chapter 4: **DISCUSSION**

Generating biochemically and biophysically tunable brain tissue models is an urgent need in neuroscience, hence there is a progressive increase in the incidence of neurodegenerative diseases. Although 2D *in vitro* models are useful for preliminary studies, they are not suitable to recapitulate the complex cellular microenvironment and communication within the central nervous system. Only one side of the cell is confronted with the cell culture medium while the other side of the cell is attached to the cell culture dish, which is much stiffer than the native tissue microenvironment. Moreover, the interactions among cells occur only in the lateral plane, which is totally different from natural cellular communication. On the other hand, *in vivo* models have also drawbacks in the neuroscience studies due to different immunologic and cellular responses received by model organisms, divergent genetic expression patterns, differences in cortical progenitor subtypes and morphological variations when it is compared with the human anatomy and pathophysiology [71]. Although the mostly used animals in neuroscience studies, including zebrafish and mouse, conserve general morphology, the discrepancies that are carried among the organisms lead to unreliable results. Ethical issues are also considerable problems for *in vivo* studies. Eventually, 3D cellular models are the most desirable choice for studying central nervous system-related diseases and molecular physiology of the brain [72, 73].

To recreate the brain microenvironment, there might be two approaches and these are scaffold-free and scaffold-based systems. When both systems are compared, it can be concluded that scaffold-based systems are more advantageous due to their tunable biochemical and biophysical properties [74]. For this purpose, natural or synthetic polymers can be used for tissue fabrication. Hydrogels, one of the frequently applied 3D models, resemble native tissue with many physical factors such as high water capacity, modulated elasticity, and mass transport features [21]. In recent studies, hydrogels were generated using ECM scaffolds and one of the most frequently applied methods to generate such scaffolds is decellularization [75].

In this study, we aimed to construct a brain hydrogel model from decellularized bovine brain tissue with tunable biochemical and biophysical properties. For this particular purpose, we examined different decellularization methods including chemical, physical, biological, and combined treatments. Up until now, there is no study showing a

decellularization protocol for bovine brain tissue meeting the gold standards of decellularization and fabricating hydrogels from bovine brain tissue.

In our study, only bovine brain cortex tissue was used whereas the cerebellum was excluded. Medberry *et al* showed the importance of tissue specificity by comparing neuron cultures in various tissue-ECM, including decellularized urinary bladder, spinal cord, and brain. Eventually, results indicate that the db-ECM promotes neurite outgrowth whereas decellularized urinary bladder and spinal cord do not provide this support to the cultured brain-derived cells [76]. Not only tissue relatedness but the importance of selecting a particular brain region was also studied [77]. Granato and his colleagues worked on the decellularization of the mouse brain using the SDS-treatment method (similar to option E in our study), and they also observed that decellularized brain tissue provides eligible microenvironment neuron cells [78]. We also showed that different db-ECM supported the neuron culture indicating expression of neuronal markers including neuronal nuclear marker NeuN and mature neuron cytoskeletal marker Beta-tubulin III. In the hydrogels which were constructed using db-ECM of methods E and G, neurite formation was observed starting on day 4.

Unquestionably, the brain is the most complex organ in the human body. This complexity relies on its heterogenous ultrastructure, outstanding mechanical properties with its soft construction and high lipid content, and the presence of grey and white matter. For the present study, the most challenging point of brain physiology was the presence of ECM proteins at low levels [6]. For this reason, the selection of the decellularization method is strikingly important as it should be supportive in retaining ECM proteins.

We could not obtain any hydrogel formation in methods A, B, and C, when we applied the indicated decellularization methods in the bovine brain tissue. Unsuccessful gelation processes were also correlated with the reduction of collagen levels. Peracetic acid and freeze-thaw cycles might have an effect on disrupting the ECM framework [79, 80]. The methods which provide successful gelation (D, E, F, and G) showed a significant increase in collagen content. Accordingly, the preservation of collagen is an important factor during decellularization as collagen provides tensile strength and joins the framework of the tissue [80]. Apart from collagen, sGAG is another important ECM constituent for native brain tissue, which mediates cellular behavior across neural networks [6, 39]. In our study, we observed the preservation of sGAG proteins in

decellularization methods A, B, and G, whereas slight reduction was examined in the other options.

Although it was reported that SDS as a decellularization agent is damaging the collagen network [79, 80], we did not encounter any harm in using SDS in decellularization methods. On the contrary, we observed a remarkable increase in collagen content due to the shrinkage of the tissue during decellularization methods D, E, F, and G, similarly, the shrinkage of the brain tissue during decellularization was also considered in other studies [77, 78].

In our study, we observed variability in stableness in hydrogel size among hydrogels created with different decellularization methods during cell viability assessments. In option D, the contraction of the hydrogel was the lowest, whereas minimum cell viability was observed in comparison to other gels. The highest rate of contraction was observed by hydrogel obtained from method F. Correspondingly, cells tend to escape from the gel, so growth out of the hydrogel was also observed in this sample. Ahearne *et.al.* showed the contraction differences in hydrogels derived from cornea tissue treated with different decellularization methods. The contraction of hydrogels and reduction in their sizes were explained by the number of viable cells and their tendency to remodel their environment through mechanical and enzymatic mechanisms [41]. Hereby, we can conclude that an optimal ratio of hydrogel contraction rate is necessary for the best cytocompatibility. In options E and G, a moderate rate of contraction was observed.

Although there are many studies concerning decellularized tissue ECM, only a small portion of studies mentioned their biophysical properties including stiffness, viscoelasticity, and elasticity. In the literature, it was stated that material characteristics have an important impact on cell and tissue growth, cell motility, and tissue homeostasis [81]. In Kingshott *et.al.*'s publication, it was postulated that matrix stiffness has a direct effect on cell behavior as cells continuously remodel the matrix [82]. In the study done by Healy *et.al.,* the self-renewal and differentiation capacities of neuronal stem cells were observed in different biochemical and physically well-defined microenvironments. The lower stiffness range (10 Pa) resulted in the inhibition of differentiation and cell spreading whereas 500 Pa resulted in neuronal differentiation and higher stiffness matrices caused glial differentiation [83]. In this study, we showed that distinct decellularization methods result in hydrogels with different mechanical properties that can mimic native tissues. In addition, the stiffness of the hydrogels obtained by rheology were in a similar range compared to hydrogels obtained from other animals [76]. Importantly, other than the

decellularization method, we also demonstrated that increasing the ligand density in sample G hydrogels from 10 to 20 mg/ml led to a more stable db-ECM gel even though the G' values were similar in sample G10 and G20 which point outs the tunability of db-ECM hydrogels. In addition, cell proliferation also seemed to be dependent on the stability and ligand density of hydrogels since the metabolic activity of cells growing in G20 hydrogels was higher than in G10 hydrogels on day 9 (*Figure* 13).

Tissues and organs demonstrate both viscous and elastic properties in response to a physical force which is called viscoelasticity. Recent studies state that ECM viscoelasticity is a crucial regulator in cell proliferation, migration as well as differentiation and there is a correlation between viscoelasticity and brain-related diseases was stated. According to Braun et.al.'s study, gender and age have a direct effect in the brain viscoelasticity [84]. Apart from aging, diseases such as multiple sclerosis were also connected to changes in brain viscoelasticity [38]. For this reason, it is crucial to identify the composition and biophysical properties of the tissue of interest in order to modulate the parameters related to the biophysical structure of the ECM depending on the application.

Here, in our knowledge for the first time, we showed that creep-response curves of bovine-brain derived hydrogels and indicate that these hydrogels are stress-relaxing materials. In particular, sample F demonstrated faster recovery compared to sample G20, and interestingly, sample G20 displayed a similar gelation curve and an end-point G' value with sample F, however, their time-dependent viscoelastic properties were distinct. We also note that this difference might explain the metabolic activity of cells grown in these mechanically distinct db-ECM gels. Recent studies also suggest that stress-relaxing ECM can induce the expression of proteolytic enzymes in cells which in turn, these enzymes remodel the matrix which might be a similar scenario we observed in db-ECM hydrogels obtained with protocol F in our study [85, 86]. Together, we can conclude that decellularization techniques on native tissues have an impact on the viscoelastic behavior of decellularized hydrogels, and characterization of mechanical properties of d-ECM hydrogels is vital since these materials recapitulate the native organs and the response of cells in a biologically relevant way.

Apart from promising advantages, there are also several disadvantages of using decellularized ECM. Batch-to-batch variability is the most possible unmanageable circumstance during decellularization applications. We also experienced difficulties in batch-to-batch variability as there are multiple parameters affecting the process.

However, optimization of decellularization steps including the incubation conditions, milling process, and pH adjustment of the decellularized digest were key steps to overcome this difficulty. At the end of the study, the amount of the digest to be neutralized, the amount of NaOH to be added, and the amount of the DMEM high glucose medium to resuspend the lyophilized neutralized digest were determined. Another drawback of using decellularized ECM is the possible weakness of the constructed structure. Synthetic materials are more operable during the construction of scaffolds [74], but using an optimal concentration of polymer content and managing the relationship between the stiffness and the polymer content are important issues to achieve successful constructs. Another gold standard of decellularization is the remnants of DNA due to the improper decellularization process, which might cause adverse immunological reactions. The surface area of tissue pieces should be small enough to react with the treatment solution. Starting volume of the tissue pieces should be small enough, so the solutions could penetrate inside the tissue. Lastly, terminal sterilization which might include ultraviolet irradiation, ethylene oxide, or supercritical carbon dioxide treatment, is an important point during applications with decellularized materials [87]. Together with this, we worked under sterile conditions after the cryo-milling process and repeated the lyophilization step to resuspend the digest in a sterile solution, so we did not require any further terminal sterilization steps. Up to 17 days of incubation, we did not encounter any contamination in the cell culture.

Although synthetic materials such as collagen or poly-ethylene glycol have many advantages during the construction of the model, the bioactivity-supporting effect of naturally derived d-ECM is compelling. For this reason, applications with decellularized ECM are promising and worth emphasizing techniques. We clearly demonstrated that different decellularization methods results in varying microenvironment conditions and the differences in the biochemical and biophysical properties cause distinction in the adaptation of the neurons to the culture environment. To analyze the effect of the 3D hydrogel platform on the adaptation of the cells further, differentiation of the neuroblastoma cells was investigated in the 3D hydrogel culture, which was constructed by the decellularized ECM derived by option E, comparing with its differentiation state on 2D culture. Neuroblastoma is a childhood cancer arising from the neural crest and it is possible to differentiate neuroblastoma cells into mature neuron phenotypes by certain agents [88].

DISCUSSION

For differentiation of the SH-SY5Y cells, different approaches were made including the gradual decrease of the serum content in the medium, the addition of retinoic acid (RA), and the addition of neurotrophic factors to the neurobasal medium. The reason behind the serum deprivation was the elimination of epithelial cells to achieve a homogenous neuronal cell population to be differentiated, whereas the SH-SY5Y cell line is a heterogenous population [89]. Until day 9 the neuronal cells were selected, so after this time point, the selected cell population was supported with several neurotrophic factors including N2, B27, KCl, and RA to be induced for neuronal maturation. RA plays a major role during neuronal differentiation by administrating complex signaling pathways such as protein kinase A-dependent pathway, transcription factors, and extracellular molecules including Wnt signaling [90]. While N2 and B27 was expected to promote neurogenesis by promoting certain signaling pathways, KCl might cause depolarization of neurons by activation of potassium channels [91, 92].

During the proceeding of the neuronal differentiation procedure, the cell proliferation was reduced, the expression of neuronal markers was distinctively changed and the morphology of the neuronal cells was altered in both 2D and 3D conditions. In 2D culture, the neuronal cells were possessing long axons, forming a synaptic network with the nearby cells (*Figure* 16). Also, the number of cells was decreased apparently, and proliferation was reduced, as this outcome was stated as an important feature of the differentiated neuronal cells. At the beginning of the differentiation trial, the number of cells should be determined carefully with the possible loss of neurons in 30-40% [47]. Also, the differentiated cells are more inclined to be affected by stress factors, so the cells should be more gently handled than the cells that are cultured as usual.

In 2D differentiated neuroblastoma cells, several changes were shown in gene expression. As expected, there was a significant increase in the mature neuron marker *TUBB3* and a significant decrease in the stemness marker *SOX2*, providing perfect signs for neuronal maturation. On the other hand, the expression of *CHAT* was elevated, so it can be concluded that there was an induction in cholinergic neuron differentiation by the applied differentiation method. Unexpectedly, the expression of the markers *MAP2* and *MAPT* was in reduced amounts which might be due to the timing of the analysis and the stage of the differentiation while the samples were collected. This condition can be supported by a study published by Przyborski *et.al*., by which it was stated that high levels of *MAP2c* mRNA transcripts in the early stages of the differentiation were reduced as the developmental progression proceeded [93]. In our study, another gene that was affected

by neuronal differentiation was *RET*, a proto-oncogene marker. Studies show that there was an increased expression of *RET* starting from day 3 of the RA treatment and this increase might stimulate neuronal differentiation [60, 94]. RET is more common in dopaminergic neurons and the increase of this gene was correlated with the promoted neurogenesis of dopaminergic neurons. Moreover, the elevation of the RET expression might be a sign of the completion of early differentiation phases [61]. Studies also showed that there might be an increase in *PSEN1* gene expression levels, but we did not encounter any significant change in *PSEN1* levels as well as *APP*, although a slight increase was observed by *PSEN1* [95].

After analyzing the differentiation of neuroblastoma cells in 2D culture, the cells were encapsulated in a hydrogel derived from db-ECM achieved through option E, and the differentiated cells were observed from similar perspectives. Similarly, neuronal network formation was clearly observed by differentiated cells (*Figure* 19), while the control groups were having cell clusters in the form of spherical clumps. Undifferentiated neuroblastoma cells behave more like cancer cells so they tend to form clumps, whereas neurogenesis was strongly induced by the treatments done during differentiation. At that point, the impact of physical confinement provided by 3D matrices on cell behavior can be clearly demonstrated. These morphological alterations were also displayed at the gene expression levels. On the contrary to the 2D differentiated cells, *SYP* levels, a synaptic marker, were significantly increased by differentiated cells on 3D matrices. Although the functionality of this gene is not completely clarified, it has important roles in the vesicular ion channel activity and vesicular endocytosis [96]. Similar results were reached out with the increased gene expression of *TUBB3* and *CHAT* and decreased levels of *MAP2*. Apart from increased levels of cholinergic neuron marker, there was also an increase in glial marker, *GFAP*. Although glial cell formation was not aimed during the differentiation procedure, due to the biomechanical characteristics of the hydrogel glial cell formation was possibly induced. In Hu *et.al.*'s study, increased expression of GFAP, due to inhibition of YAP, was shown in 3D soft matrices (~42 Pa), while there was inhibited expression in the 3D stiff environments (~990 Pa) where stiffness was tuned via modulating concentration of calcium added to the alginate content [97].

Chapter 5: **CONCLUSION AND OUTLOOK**

In neuroscience studies, mimicking the body's most complex organ, the brain, has always been a challenge. 2D culture models are not satisfactory due to many reasons including improper signaling pathways and inadequate cellular interactions in an unrestricted volume which is unrelated to biomechanical features. Similarly, in vivo studies have major disadvantages such as different physiological properties than human brain. For this reason, a 3D tissue model hosting human-derived cells might be the perfect candidate model for neuroscience studies. Accordingly, decellularized tissue provides maximum resemblance to the in vivo ECM which can be used for construction of hydrogels.

In the present study, we evaluated different decellularization methods, including chemical, physical, and biological approaches which were applied to the bovine brain tissue. In this regard, we established that the method which was based on SDS treatment was the most effective for hydrogel generation which also supported neuron culture. During optimization of decellularization methods, the findings suggested that the conservation of biochemical content, some of which were collagen and sGAG could be an important point for gelation during decellularization. Each treatment resulted in a different biochemical and biophysical composition of the tissue. Within this context, viscoelasticity and stiffness have an important impact on neuronal culture, as neurite formation differed in hydrogels with varying biochemical and biophysical properties.

In the second part of the study, the constructed hydrogel model which was derived from db-ECM was examined for neuroblastoma cell differentiation. In the differentiation regime, RA was applied with the gradual decrease of the serum content and the cell medium was subsequently supplied with several neurotrophic factors. The differentiation process proceeded distinctively in the 3D hydrogel matrix in comparison to 2D culture, whereas the 3D culture system mimics the natural tissue environment with outstanding biochemical and biomechanical properties.

Since one of the major issues within the neurodegenerative disease progression is the change in brain viscoelasticity and stiffness, this hydrogel model might be promising approach to modulate the pathophysiology of Alzheimer's disease. This study highlights the importance of neuron-culture-favorable hydrogel derived from db-ECM. Further investigations are needed to examine these hydrogels based on their adaptability to

applications in various neurodegenerative disease and tumor models, in which the biochemical and biomechanical changes might be modulated.

BIBLIOGRAPHY

1. Karamanos, N.K., et al., *A guide to the composition and functions of the extracellular matrix.* FEBS J, 2021. **288**(24): p. 6850-6912.
2. Frantz, C., K.M. Stewart, and V.M. Weaver, *The extracellular matrix at a glance.* Journal of cell science, 2010. **123**(Pt 24): p. 4195-4200.
3. Nicolas, J., et al., *3D extracellular matrix mimics: fundamental concepts and role of materials chemistry to influence stem cell fate.* Biomacromolecules, 2020. **21**(6): p. 1968-1994.
4. Rauti, R., N. Renous, and B.M. Maoz, *Mimicking the brain extracellular matrix in vitro: a review of current methodologies and challenges.* Israel Journal of Chemistry, 2020. **60**(12): p. 1141-1151.
5. Bonneh-Barkay, D. and C.A. Wiley, *Brain extracellular matrix in neurodegeneration.* Brain pathology, 2009. **19**(4): p. 573-585.
6. Sood, D., et al., *Fetal brain extracellular matrix boosts neuronal network formation in 3D bioengineered model of cortical brain tissue.* ACS biomaterials science & engineering, 2016. **2**(1): p. 131-140.
7. Ruoslahti, E., *Brain extracellular matrix.* Glycobiology, 1996. **6**(5): p. 489-492.
8. Baiguera, S., et al., *Electrospun gelatin scaffolds incorporating rat decellularized brain extracellular matrix for neural tissue engineering.* Biomaterials, 2014. **35**(4): p. 1205-1214.
9. Xu, L., A. Nirwane, and Y. Yao, *Basement membrane and blood–brain barrier.* Stroke and vascular neurology, 2019. **4**(2).
10. Hall, C.M., E. Moeendarbary, and G.K. Sheridan, *Mechanobiology of the brain in ageing and Alzheimer's disease.* European Journal of Neuroscience, 2021. **53**(12): p. 3851-3878.
11. Lau, L.W., et al., *Pathophysiology of the brain extracellular matrix: a new target for remyelination.* Nature Reviews Neuroscience, 2013. **14**(10): p. 722-729.
12. Reiter, N., et al., *Insights into the Microstructural Origin of Brain Viscoelasticity.* Journal of Elasticity, 2021. **145**(1): p. 99-116.
13. Peruffo, A. and B. Cozzi, *Bovine brain: an in vitro translational model in developmental neuroscience and neurodegenerative research.* Frontiers in pediatrics, 2014. **2**: p. 74.
14. Chiti, M.C., et al., *Ovarian extracellular matrix-based hydrogel for human ovarian follicle survival in vivo: A pilot work.* Journal of Biomedical Materials Research Part B: Applied Biomaterials, 2022. **110**(5): p. 1012-1022.
15. Ercan, H., A.E. Elçin, and Y.M. Elçin, *Assessment of dopamine-conjugated decellularized bovine tendon extracellular matrix as a bioadhesive.* Materials Today Communications, 2022. **31**: p. 103634.
16. Kundu, J., et al., *Decellularized retinal matrix: natural platforms for human retinal progenitor cell culture.* Acta biomaterialia, 2016. **31**: p. 61-70.
17. Ozudogru, E., et al., *Decellularized spinal cord meninges extracellular matrix hydrogel that supports neurogenic differentiation and vascular structure formation.* Journal of Tissue Engineering and Regenerative Medicine, 2021. **15**(11): p. 948-963.
18. Beachley, V., et al., *Extracellular matrix particle–glycosaminoglycan composite hydrogels for regenerative medicine applications.* Journal of Biomedical Materials Research Part A, 2018. **106**(1): p. 147-159.

19. Fiore, N.J., et al., *3D biocomposite culture enhances differentiation of dopamine-like neurons from SH-SY5Y cells: A model for studying Parkinson's disease phenotypes.* Biomaterials, 2022. **290**: p. 121858.
20. Baek, J., et al., *Egr1 is a 3D matrix–specific mediator of mechanosensitive stem cell lineage commitment.* Science advances, 2022. **8**(15): p. eabm4646.
21. Wilson, J.L. and T.C. McDevitt, *Biofunctional hydrogels for Three-dimensional stem cell culture*, in *Biology and Engineering of Stem Cell Niches*. 2017, Elsevier. p. 345-362.
22. Lu, H., et al., *Comparison of decellularization techniques for preparation of extracellular matrix scaffolds derived from three-dimensional cell culture.* Journal of Biomedical Materials Research Part A, 2012. **100**(9): p. 2507-2516.
23. Gilbert, T.W., T.L. Sellaro, and S.F. Badylak, *Decellularization of tissues and organs.* Biomaterials, 2006. **27**(19): p. 3675-3683.
24. Gilpin, A. and Y. Yang, *Decellularization Strategies for Regenerative Medicine: From Processing Techniques to Applications.* BioMed research international, 2017. **2017**: p. 9831534-9831534.
25. Fu, R.-H., et al., *Decellularization and recellularization technologies in tissue engineering.* Cell transplantation, 2014. **23**(4-5): p. 621-630.
26. Sackett, S.D., et al., *Extracellular matrix scaffold and hydrogel derived from decellularized and delipidized human pancreas.* Scientific Reports, 2018. **8**(1): p. 10452.
27. Cramer, M.C. and S.F. Badylak, *Extracellular matrix-based biomaterials and their influence upon cell behavior.* Annals of biomedical engineering, 2020. **48**(7): p. 2132-2153.
28. Zhang, W., et al., *Research progress in decellularized extracellular matrix-derived hydrogels.* Regenerative Therapy, 2021. **18**: p. 88-96.
29. Badylak, S.F., D.O. Freytes, and T.W. Gilbert, *Extracellular matrix as a biological scaffold material: Structure and function.* Acta biomaterialia, 2009. **5**(1): p. 1-13.
30. Freytes, D.O., et al., *Preparation and rheological characterization of a gel form of the porcine urinary bladder matrix.* Biomaterials, 2008. **29**(11): p. 1630-1637.
31. Saldin, L.T., et al., *Extracellular matrix hydrogels from decellularized tissues: Structure and function.* Acta biomaterialia, 2017. **49**: p. 1-15.
32. Vining, K.H. and D.J. Mooney, *Mechanical forces direct stem cell behaviour in development and regeneration.* Nature reviews Molecular cell biology, 2017. **18**(12): p. 728-742.
33. Tyler, W.J., *The mechanobiology of brain function.* Nature Reviews Neuroscience, 2012. **13**(12): p. 867-878.
34. Wuerfel, J., et al., *MR-elastography reveals degradation of tissue integrity in multiple sclerosis.* Neuroimage, 2010. **49**(3): p. 2520-2525.
35. Lipp, A., et al., *Progressive supranuclear palsy and idiopathic Parkinson's disease are associated with local reduction of in vivo brain viscoelasticity.* European radiology, 2018. **28**(8): p. 3347-3354.
36. Streitberger, K.-J., et al., *High-resolution mechanical imaging of glioblastoma by multifrequency magnetic resonance elastography.* PloS one, 2014. **9**(10): p. e110588.
37. Gerischer, L.M., et al., *Combining viscoelasticity, diffusivity and volume of the hippocampus for the diagnosis of Alzheimer's disease based on magnetic resonance imaging.* NeuroImage: Clinical, 2018. **18**: p. 485-493.

38. Streitberger, K.-J., et al., *Brain viscoelasticity alteration in chronic-progressive multiple sclerosis.* PloS one, 2012. **7**(1): p. e29888.
39. DeQuach, J.A., et al., *Decellularized porcine brain matrix for cell culture and tissue engineering scaffolds.* Tissue Engineering Part A, 2011. **17**(21-22): p. 2583-2592.
40. Gaetani, R., et al., *Evaluation of different decellularization protocols on the generation of pancreas-derived hydrogels.* Tissue Engineering Part C: Methods, 2018. **24**(12): p. 697-708.
41. Fernández-Pérez, J. and M. Ahearne, *The impact of decellularization methods on extracellular matrix derived hydrogels.* Scientific reports, 2019. **9**(1): p. 1-12.
42. White, L.J., et al., *The impact of detergents on the tissue decellularization process: a ToF-SIMS study.* Acta biomaterialia, 2017. **50**: p. 207-219.
43. Seo, Y., et al., *Development of an Anisotropically Organized Brain dECM Hydrogel-Based 3D Neuronal Culture Platform for Recapitulating the Brain Microenvironment in Vivo.* ACS Biomaterials Science & Engineering, 2020. **6**(1): p. 610-620.
44. Koh, I., et al., *The mode and dynamics of glioblastoma cell invasion into a decellularized tissue-derived extracellular matrix-based three-dimensional tumor model.* Scientific reports, 2018. **8**(1): p. 1-12.
45. Biedler, J.L., et al., *Multiple neurotransmitter synthesis by human neuroblastoma cell lines and clones.* Cancer research, 1978. **38**(11_Part_1): p. 3751-3757.
46. Barth, M., et al., *Quantitative proteomics and in-cell cross-linking reveal cellular reorganisation during early neuronal differentiation of SH-SY5Y cells.* Communications Biology, 2022. **5**(1): p. 1-16.
47. Shipley, M.M., C.A. Mangold, and M.L. Szpara, *Differentiation of the SH-SY5Y human neuroblastoma cell line.* JoVE (Journal of Visualized Experiments), 2016(108): p. e53193.
48. Qiao, J., et al., *PI3K/AKT and ERK regulate retinoic acid-induced neuroblastoma cellular differentiation.* Biochemical and Biophysical Research Communications, 2012. **424**(3): p. 421-426.
49. Bottenstein, J.E. and G.H. Sato, *Growth of a rat neuroblastoma cell line in serum-free supplemented medium.* Proceedings of the National Academy of Sciences, 1979. **76**(1): p. 514-517.
50. Sünwoldt, J., et al., *Neuronal Culture Microenvironments Determine Preferences in Bioenergetic Pathway Use.* Front Mol Neurosci, 2017. **10**: p. 305.
51. Xie, H.-r., L.-s. Hu, and G.-y. Li, *SH-SY5Y human neuroblastoma cell line: in vitro cell model of dopaminergic neurons in Parkinson's disease.* Chinese medical journal, 2010. **123**(08): p. 1086-1092.
52. Dehmelt, L. and S. Halpain, *The MAP2/Tau family of microtubule-associated proteins.* Genome Biology, 2004. **6**(1): p. 204.
53. Kaech, S., B. Ludin, and A. Matus, *Cytoskeletal plasticity in cells expressing neuronal microtubule-associated proteins.* Neuron, 1996. **17**(6): p. 1189-1199.
54. Katsetos, C.D., M.M. Herman, and S.J. Mörk, *Class III β-tubulin in human development and cancer.* Cell motility and the cytoskeleton, 2003. **55**(2): p. 77-96.
55. Gusel'nikova, V.V. and D.E. Korzhevskiy, *NeuN As a Neuronal Nuclear Antigen and Neuron Differentiation Marker.* Acta Naturae, 2015. **7**(2): p. 42-7.
56. Cassiman, D., et al., *Synaptophysin: A Novel Marker for Human and Rat Hepatic Stellate Cells.* The American Journal of Pathology, 1999. **155**(6): p. 1831-1839.

57. White, D.N. and M.H. Stowell, *Room for Two: The Synaptophysin/Synaptobrevin Complex.* Frontiers in Synaptic Neuroscience, 2021: p. 47.
58. Graham, V., et al., *SOX2 Functions to Maintain Neural Progenitor Identity.* Neuron, 2003. **39**(5): p. 749-765.
59. Bunone, G., et al., *Induction of RET Proto-Oncogene Expression in Neuroblastoma Cells Precedes Neuronal Differentiation and Is Not Mediated by Protein Synthesis.* Experimental Cell Research, 1995. **217**(1): p. 92-99.
60. Tahira, T., et al., *Expression of the ret proto-oncogene in human neuroblastoma cell lines and its increase during neuronal differentiation induced by retinoic acid.* Oncogene, 1991. **6**(12): p. 2333-2338.
61. Barth, M., et al., *Quantitative proteomics and in-cell cross-linking reveal cellular reorganisation during early neuronal differentiation of SH-SY5Y cells.* Communications Biology, 2022. **5**(1): p. 551.
62. Oda, Y., *Choline acetyltransferase: the structure, distribution and pathologic changes in the central nervous system.* Pathol Int, 1999. **49**(11): p. 921-37.
63. Yang, Z. and K.K. Wang, *Glial fibrillary acidic protein: from intermediate filament assembly and gliosis to neurobiomarker.* Trends Neurosci, 2015. **38**(6): p. 364-74.
64. Müller, U.C., T. Deller, and M. Korte, *Not just amyloid: physiological functions of the amyloid precursor protein family.* Nature Reviews Neuroscience, 2017. **18**(5): p. 281-298.
65. Bagaria, J., E. Bagyinszky, and S.S.A. An, *Genetics, Functions, and Clinical Impact of Presenilin-1 (PSEN1) Gene.* International Journal of Molecular Sciences, 2022. **23**(18): p. 10970.
66. Yi, H.-G., et al., *A bioprinted human-glioblastoma-on-a-chip for the identification of patient-specific responses to chemoradiotherapy.* Nature biomedical engineering, 2019. **3**(7): p. 509-519.
67. Hong, J.Y., et al., *Decellularized brain matrix enhances macrophage polarization and functional improvements in rat spinal cord injury.* Acta biomaterialia, 2020. **101**: p. 357-371.
68. Lam, D., et al., *Tissue-specific extracellular matrix accelerates the formation of neural networks and communities in a neuron-glia co-culture on a multi-electrode array.* Scientific reports, 2019. **9**(1): p. 1-15.
69. Simsa, R., et al., *Brain organoid formation on decellularized porcine brain ECM hydrogels.* PloS one, 2021. **16**(1): p. e0245685.
70. Lin, T., et al., *Hydrogel derived from porcine decellularized nerve tissue as a promising biomaterial for repairing peripheral nerve defects.* Acta Biomaterialia, 2018. **73**: p. 326-338.
71. Roth, J.G., et al., *Advancing models of neural development with biomaterials.* Nature Reviews Neuroscience, 2021. **22**(10): p. 593-615.
72. McCrary, M.W., et al., *Decellularized tissues as platforms for in vitro modeling of healthy and diseased tissues.* Acta Biomaterialia, 2020. **111**: p. 1-19.
73. Kajtez, J., et al., *3D biomaterial models of human brain disease.* Neurochemistry International, 2021. **147**: p. 105043.
74. Yildirimer, L., et al., *Engineering three-dimensional microenvironments towards in vitro disease models of the central nervous system.* Biofabrication, 2019. **11**(3): p. 032003.
75. Zilberman, A. and R.C. Cornelison, *Microphysiological models of the central nervous system with fluid flow.* Brain Research Bulletin, 2021. **174**: p. 72-83.

76. Medberry, C.J., et al., *Hydrogels derived from central nervous system extracellular matrix.* Biomaterials, 2013. **34**(4): p. 1033-1040.
77. Reginensi, D., et al., *Role of region-specific brain decellularized extracellular matrix on in vitro neuronal maturation.* Tissue Engineering Part A, 2020. **26**(17-18): p. 964-978.
78. Granato, A.E.C., et al., *A novel decellularization method to produce brain scaffolds.* Tissue and Cell, 2020. **67**: p. 101412.
79. Crapo, P.M., T.W. Gilbert, and S.F. Badylak, *An overview of tissue and whole organ decellularization processes.* Biomaterials, 2011. **32**(12): p. 3233-3243.
80. Zhang, X., et al., *Decellularized extracellular matrix scaffolds: Recent trends and emerging strategies in tissue engineering.* Bioactive Materials, 2022. **10**: p. 15-31.
81. Mierke, C.T., *Viscoelasticity, Like Forces, Plays a Role in Mechanotransduction.* Frontiers in Cell and Developmental Biology, 2022. **10**.
82. Sasikumar, S., et al., *Decellularized extracellular matrix hydrogels—cell behavior as a function of matrix stiffness.* Current Opinion in Biomedical Engineering, 2019. **10**: p. 123-133.
83. Saha, K., et al., *Substrate Modulus Directs Neural Stem Cell Behavior.* Biophysical Journal, 2008. **95**(9): p. 4426-4438.
84. Sack, I., et al., *The impact of aging and gender on brain viscoelasticity.* Neuroimage, 2009. **46**(3): p. 652-657.
85. Varedi, M., et al., *Stress-relaxation and contraction of a collagen matrix induces expression of TGF-β and triggers apoptosis in dermal fibroblasts.* Biochemistry and Cell Biology, 2000. **78**(4): p. 427-436.
86. Nam, S., et al., *Strain-enhanced stress relaxation impacts nonlinear elasticity in collagen gels.* Proceedings of the National Academy of Sciences, 2016. **113**(20): p. 5492-5497.
87. Yaldiz, B., et al., *Effect of sterilization methods on the mechanical stability and extracellular matrix constituents of decellularized brain tissues.* The Journal of Supercritical Fluids, 2021. **175**: p. 105299.
88. Cai, A., et al., *Neuroblastoma SH-SY5Y Cell Differentiation to Mature Neuron by AM580 Treatment.* Neurochemical Research, 2022. **47**(12): p. 3723-3732.
89. Bell, N., et al., *Store-operated Ca2+ entry in proliferating and retinoic acid-differentiated N- and S-type neuroblastoma cells.* Biochimica et Biophysica Acta (BBA) - Molecular Cell Research, 2013. **1833**(3): p. 643-651.
90. Dhara, S.K. and S.L. Stice, *Neural differentiation of human embryonic stem cells.* Journal of cellular biochemistry, 2008. **105**(3): p. 633-640.
91. Yang, T. *KCl-induced depolarization facilitates neuronal differentiation of P19 embryonic carcinoma cells*. 2013.
92. Lasher, R.S. and I.S. Zagon, *The effect of potassium on neuronal differentiation in cultures of dissociated newborn rat cerebellum.* Brain Research, 1972. **41**(2): p. 482-488.
93. Przyborski, S.A. and M.A. Cambray-Deakin, *Developmental regulation of MAP2 variants during neuronal differentiation in vitro.* Brain Res Dev Brain Res, 1995. **89**(2): p. 187-201.
94. Forster, J.I., et al., *Characterization of Differentiated SH-SY5Y as Neuronal Screening Model Reveals Increased Oxidative Vulnerability.* SLAS Discovery, 2016. **21**(5): p. 496-509.

95. de Medeiros, L.M., et al., *Cholinergic Differentiation of Human Neuroblastoma SH-SY5Y Cell Line and Its Potential Use as an In vitro Model for Alzheimer's Disease Studies.* Molecular Neurobiology, 2019. **56**(11): p. 7355-7367.
96. White, D.N. and M.H.B. Stowell, *Room for Two: The Synaptophysin/Synaptobrevin Complex.* Front Synaptic Neurosci, 2021. **13**: p. 740318.
97. Hu, Y., et al., *Matrix stiffness changes affect astrocyte phenotype in an in vitro injury model.* NPG Asia Materials, 2021. **13**(1): p. 35.